A mixed virtual element method for a pseudostress-based formulation of linear elasticity*

Ernesto Cáceres† Gabriel N. Gatica‡ Filánder A. Sequeira§

Abstract

In this paper we introduce and analyze a mixed virtual element method (mixed-VEM) for a pseudostress-displacement formulation of the linear elasticity problem with non-homogeneous Dirichlet boundary conditions. We follow a previous work by some of the authors, and employ a mixed formulation that does not require symmetric tensor spaces in the finite element discretization. More precisely, the main unknowns here are given by the pseudostress and the displacement, whereas other physical quantities such as the stress, the strain tensor of small deformations, and the rotation, are computed through simple postprocessing formulae in terms of the pseudostress variable. We first recall the corresponding variational formulation, and then summarize the main mixed-VEM ingredients that are required for our discrete analysis. In particular, we utilize a well-known local projector onto a suitable polynomial subspace to define a calculable version of our discrete bilinear form, whose continuous version requires information of the variables on the interior of each element. Next, we show that the global discrete bilinear form satisfies the hypotheses required by the Babuška-Brezzi theory. In this way, we conclude the well-posedness of our mixed-VEM scheme and derive the associated *a priori* error estimates for the virtual solutions as well as for the fully computable projections of them. Furthermore, we also introduce a second element-by-element postprocessing formula for the pseudostress, which yields an optimally convergent approximation of this unknown with respect to the broken $\mathbb{H}(\mathbf{div})$-norm. In addition, this postprocessing formula can also be applied to the postprocessed stress tensor. Finally, several numerical results illustrating the good performance of the method and confirming the theoretical rates of convergence are presented.

Key words: pseudostress-displacement formulation, linear elasticity, mixed virtual element method, a priori error analysis, postprocessing techniques

1 Introduction

The virtual element method (VEM), which was first introduced and analyzed in [4] using the Poisson problem as a model, arised as a natural consequence of new developments and interpretations of

*This work was partially supported by CONICYT-Chile through BASAL project CMM, Universidad de Chile, project Anillo ACT1118 (ANANUM), and the Becas-CONICYT Programme for foreign students; by Centro de Investigación en Ingeniería Matemática (CI^{2}MA), Universidad de Concepción; and by Universidad Nacional (Costa Rica), through the project 0106-16.

†CI^{2}MA and Departamento de Ingeniería Matemática, Universidad de Concepción, Casilla 160-C, Concepción, Chile, email: ecaceresv@udec.cl. Present Address: Division of Applied Mathematics, Brown University, Providence, RI 02912, USA. email: ernesto_caceres_valenzuela@brown.edu

‡CI^{2}MA and Departamento de Ingeniería Matemática, Universidad de Concepción, Casilla 160-C, Concepción, Chile, email: ggatica@ci2ma.udec.cl.

§Escuela de Matemática, Universidad Nacional, Campus Omar Dengo, Heredia, Costa Rica, email: filander.sequeira@una.cr.

the mimetic finite difference method (MFDM). In fact, this new approach features the utilization of a virtual discrete space defined on a mesh made of convex or non-convex polygonal or polyhedral elements, along with the incorporation of approximate bilinear and linear forms. More precisely, the latters, being usually defined in terms of suitably chosen projectors, mimic the respective original forms, but still provide consistence and stability of the resulting modified discrete scheme. The concept *virtual* employed here means that the corresponding basis functions do not need to be known explicitly, but only the degrees of freedom defining them uniquely on each element are required. Among its main advantages, it is highlighted the fact that VEM constitutes an extension of the classical finite element technique to more general meshes, as well as a generalization of the MFDM to arbitrary degrees of accuracy and continuity properties. Other benefits of VEM, when compared with finite volume methods, MFDM, and related techniques, refer to the solid mathematical ground involved, the simplicity of the respective computational implementation, the high order approximation properties of the virtual element subspaces employed, and the consequent good quality of the numerical results provided. Furthermore, while the virtual element schemes were originally defined in terms of projectors that were ad-hoc to the problem under consideration, it is important to remark that a systematic use of the simple L^2-projection operator was recently introduced in [1] and [8].

Further interesting contributions on VEM for boundary value problems in continuum mechanics include, among others, a stream function-based approach for the classical velocity-pressure formulation of the Stokes problem in [2], a displacement-based VEM for compressible and nearly incompressible 2D and 3D linear elasticity in [5] and [16], and a VEM based on the Kirchhoff–Love formulation for linear plate bending problems in [12]. Moreover, regarding the applicability of VEM to nonlinear models, we highlight that a family of corresponding methods for the two-dimensional Navier-Stokes equations is introduced and analyzed in [10], which constitutes, up to our knowledge, the first paper applying this technique to a nonlinear model.

On the other hand, within the context of what are called mixed virtual element methods (mixed-VEM), that is those based on dual-mixed variational formulations instead of primal or primal-mixed ones, we stress that the first approach in this direction is introduced and analyzed in [11] by using the Darcy problem for fluid flow in porous media as a model. Similarly as in [4], polygonal or polyhedral elements were considered in [11], but only an approximation of the main bilinear form was needed to obtain a consistent and stable discrete scheme. In addition, taking advantage of the structure of the exact solution, a projection onto a space of restricted polynomial vector fields is introduced and employed there. Later on, further extensions of the mixed-VEM are developed in [6], [7], and [13]. In particular, edge and face VEM spaces in 2D and 3D were developed in [6], whereas [7] generalizes the results of [6] to the case of variable coefficients. In turn, a mixed-VEM for a pseudostress-based formulation of the Stokes problem is introduced and analyzed in [13]. In this work, the pseudostress and the velocity are the only unknowns, whereas the pressure is computed via a postprocessing formula. Thus, a new local projector onto a suitable space of polynomials is presented, which takes into account the main features of the continuous solution and allows the explicit integration of the terms involving the deviatoric tensors. The resulting family of local projectors is shown to be uniformly bounded, and its approximation properties are also established there.

For additional contributions on mixed-VEM for pseudostress-based formulations of boundary value problems, we begin by referring to [14] where two mixed virtual element methods are proposed for the two-dimensional Brinkman problem originally studied in [18]. Indeed, following [18], the equilibrium equation and the incompressibility condition are first used in [14] to eliminate both the velocity and the pressure, thus yielding the pseudostress as the only unknown of the resulting dual-mixed formulation. Thus, the aforementioned two schemes are determined by each one of the following projectors: the particular local one introduced in [13], and the general L^2-orthogonal projection analyzed in [6] (see also [7]). More recently, the analysis and results from [13] and [14] were extended in [15] to the case

of quasi-Newtonian Stokes flows, for which the problem originally studied in [23] was considered as a model, and hence, up to our knowledge, [15] constitutes the first work applying mixed-VEM to a nonlinear problem. While the original unknowns in [15] are given by the pseudostress, the velocity, and the pressure, the latter is eliminated by using the incompressibility condition, and in order to handle the nonlinearity involved, the velocity gradient is set as an auxiliary one. Additionally, the approach from [14] was generalized in [24] to the nonlinear Brinkman model considered in [19], whereas a mixed-VEM for a pseudostress-velocity formulation of the two-dimensional Navier-Stokes equations with Dirichlet boundary conditions is proposed and analyzed in [25]. Actually, besides projectors commonly utilized for related models, the main novelty of the method introduced in [25] is given by the simultaneous use of VEM and mixed-VEM techniques for approximating the velocity and the pseudostress, respectively. More precisely, a dual-mixed approach based on the introduction of a nonlinear pseudostress linking the usual linear one for the Stokes equations and the convective term, is employed in [25]. In this way, the aforementioned new tensor together with the velocity constitute the only unknowns of the problem, whereas the pressure is computed via a postprocessing formula. Finally, concerning the applicability of mixed-VEM to the classical linear elasticity problem, we are just aware of [3] where a low-order scheme, with a priori symmetric Cauchy stresses, was proposed and analyzed for the 2D case. In fact, the VEM concept is applied here only to the stress field by using three traction degrees of freedom per each edge, similarly to the construction of the discrete velocity field for the Stokes problem in [9], while the displacement field inside each element is essentially approximated by a rigid body motion.

According to the foregoing discussion, and in order to, on one hand, additionally contribute in the direction drawn by [13], [14], [15], [24], and [25], and on the other hand, provide an alternative to the stress-based approach from [3], we now aim to further extend the applicability of the mixed-VEM to boundary value problems in continuum mechanics, particularly in elasticity. More precisely, we consider the same pseudostress-displacement formulation introduced and analyzed in [21] (see also [20]), and develop a new mixed-VEM for the two-dimensional linear elasticity problem with non-homogeneous Dirichlet boundary conditions. Besides the fact that no symmetry is needed for the pseudostress, we highlight that the present approach yields much more freedom than [3] for choosing the virtual element subspace approximating the pseudostress and the piecewise polynomial subspace where the discrete displacement lives now, which, in turn, allows for rates of convergence of higher order. Moreover, we remark in advance that the method to be proposed here leads to fully computable element-by-element postprocessing formulae for the pseudostress as well as for the stress.

The rest of this work is organized as follows. In Section 2 we introduce the boundary value problem of interest, and recall from [21] its pseudostress-displacement mixed formulation and the associated well-posedness result. Then, in Section 3 we follow [11], [13], and [14], and introduce and analyze the virtual element method that will be employed. This includes the assumptions on the polygonal mesh, the definition of the local virtual element subspaces, the definition of the corresponding discrete bilinear forms, and certainly the resulting discrete scheme itself. Also, the interpolants and projectors to be used are introduced here, along with their approximation properties. Finally, a priori error estimates and corresponding rates of convergence for the approximations of both the pseudostress and the displacement are derived. Next, in Section 4 we follow [21] and [14], and introduce two different fully computable approximations for the pseudostress $\boldsymbol{\rho}$ and the stress $\boldsymbol{\sigma}$, for which their a priori error estimates and rates of convergence are also established. In particular, we show that the second pair of computable approximations lead to optimal rates of convergence in the broken $\mathbb{H}(\mathbf{div})$-norm. Finally, numerical experiments showing the good performance of the method with different values of the parameters and polynomial degrees involved, confirming the rates of convergence and illustrating the acurateness of the approximate solutions, are reported in Section 5.

Notations

We end the present section by providing some notations to be used along the paper, including those already employed above. Indeed, given a bounded domain $\Omega \subseteq \mathrm{R}^2$ with boundary Γ, we let $\boldsymbol{n}$ be the outward unit normal vector on Γ. In addition, standard terminology will be adopted for Lebesgue spaces $\mathrm{L}^p(\Omega)$, $p > 1$, and Sobolev spaces $\mathrm{H}^s(\Omega)$, $s \in \mathrm{R}$, with norm $\|\cdot\|_{s,\Omega}$ and seminorm $|\cdot|_{s,\Omega}$. In particular, $\mathrm{H}^{1/2}(\Gamma)$ is the space of traces of functions of $\mathrm{H}^1(\Omega)$, and $\mathrm{H}^{-1/2}(\Gamma)$ denotes its dual. We will denote by $\mathbf{M}$ and $\mathbb{M}$, the corresponding vector and tensor counterparts of the generic scalar functional space M, respectively. Then, letting $\mathbf{div}$ (resp. $\mathbf{rot}$) be the usual divergence operator div (resp. rotational operator rot) acting along the rows of a given tensor, we recall that the spaces

$$\mathbb{H}(\mathbf{div};\Omega) := \left\{ \boldsymbol{\tau} \in \mathbb{L}^2(\Omega) \ : \quad \mathbf{div}(\boldsymbol{\tau}) \in \mathbf{L}^2(\Omega) \right\}$$

and

$$\mathbb{H}(\mathbf{rot};\Omega) := \left\{ \boldsymbol{\tau} \in \mathbb{L}^2(\Omega) \ : \quad \mathbf{rot}(\boldsymbol{\tau}) \in \mathbf{L}^2(\Omega) \right\},$$

equipped with the usual norms

$$\|\boldsymbol{\tau}\|^2_{\mathbf{div};\Omega} := \|\boldsymbol{\tau}\|^2_{0,\Omega} + \|\mathbf{div}(\boldsymbol{\tau})\|^2_{0,\Omega} \qquad \forall\, \boldsymbol{\tau} \in \mathbb{H}(\mathbf{div};\Omega),$$

and

$$\|\boldsymbol{\tau}\|^2_{\mathbf{rot};\Omega} := \|\boldsymbol{\tau}\|^2_{0,\Omega} + \|\mathbf{rot}(\boldsymbol{\tau})\|^2_{0,\Omega} \qquad \forall\, \boldsymbol{\tau} \in \mathbb{H}(\mathbf{rot};\Omega),$$

are Hilbert spaces. Also, given $\boldsymbol{\tau} := (\tau_{ij})$, $\boldsymbol{\zeta} := (\zeta_{ij}) \in \mathrm{R}^{2\times 2}$, we write as usual

$$\boldsymbol{\tau}^{\mathtt{t}} := (\tau_{ji}), \qquad \mathrm{tr}(\boldsymbol{\tau}) := \sum_{i=1}^{2} \tau_{ii}, \qquad \boldsymbol{\tau}^{\mathrm{d}} := \boldsymbol{\tau} - \frac{1}{2}\mathrm{tr}(\boldsymbol{\tau})\,\mathbb{I}, \quad \text{and} \quad \boldsymbol{\tau} : \boldsymbol{\zeta} := \sum_{i,j=1}^{2} \tau_{ij}\zeta_{ij},$$

where $\mathbb{I}$ is the identity matrix of $\mathrm{R}^{2\times 2}$. Finally, in what follows we employ $\mathbf{0}$ to denote a generic null vector, null tensor or null operator, and use C, with or without subscripts, bars, tildes or hats, to denote generic constants independent of the discretization parameters, which may take different values at different places.

2 The elasticity problem and its pseudostress-based formulation

Let Ω be a bounded and simply connected polyhedral domain in R^2 with boundary Γ. Our goal is to determine the displacement $\mathbf{u}$ and the stress tensor $\boldsymbol{\sigma}$ of a linear elastic material occupying the region Ω. In other words, given a volume force $\mathbf{f} \in \mathbf{L}^2(\Omega)$ and a Dirichlet datum $\mathbf{g} \in \mathbf{H}^{1/2}(\Gamma)$, we seek a symmetric tensor field $\boldsymbol{\sigma}$ and a vector field $\mathbf{u}$ such that

$$\boldsymbol{\sigma} = \mathcal{C}\,\mathbf{e}(\mathbf{u}) \quad \text{in} \quad \Omega, \quad \mathbf{div}(\boldsymbol{\sigma}) = -\mathbf{f} \quad \text{in} \quad \Omega, \quad \text{and} \quad \mathbf{u} = \mathbf{g} \quad \text{on} \quad \Gamma, \tag{2.1}$$

where $\mathbf{e}(\mathbf{u}) := \frac{1}{2}(\nabla\,\mathbf{u} + (\nabla\,\mathbf{u})^{\mathtt{t}})$ is the strain tensor of small deformations (symmetric part of the displacement gradient), and $\mathcal{C}$ is the elasticity operator governed by Hooke's law:

$$\mathcal{C}\boldsymbol{\zeta} := 2\mu\,\boldsymbol{\zeta} + \lambda\,\mathrm{tr}(\boldsymbol{\zeta})\,\mathbb{I} \qquad \forall\, \boldsymbol{\zeta} \in \mathbb{L}^2(\Omega),$$

with λ, $\mu > 0$ being the corresponding Lamé constants.

On the other hand, from [20, 21] we know that the stress-displacement formulation of (2.1) can be re-written as: find a non-symmetric tensor $\boldsymbol{\rho}$ (pseudostress) and a vector $\mathbf{u}$ (displacement) such that

$$\boldsymbol{\rho} = \widetilde{\mathcal{C}}\,\nabla\mathbf{u} \quad \text{in} \quad \Omega, \quad \mathbf{div}(\boldsymbol{\rho}) = -\mathbf{f} \quad \text{in} \quad \Omega, \quad \text{and} \quad \mathbf{u} = \mathbf{g} \quad \text{on} \quad \Gamma, \tag{2.2}$$

where, $\widetilde{\mathcal{C}}$ is given by

$$\widetilde{\mathcal{C}}\boldsymbol{\zeta} \;:=\; \mu\,\boldsymbol{\zeta} \;+\; (\lambda+\mu)\,\mathrm{tr}(\boldsymbol{\zeta})\,\mathbb{I} \qquad \forall\,\boldsymbol{\zeta} \,\in\, \mathbb{L}^2(\Omega)\,,$$

and satisfies

$$\widetilde{\mathcal{C}}^{-1}\boldsymbol{\zeta} \,:=\, \frac{1}{\mu}\left\{\boldsymbol{\zeta} \,-\, \frac{\lambda+\mu}{2\lambda+3\mu}\,\mathrm{tr}(\boldsymbol{\zeta})\,\mathbb{I}\right\} \qquad \forall\,\boldsymbol{\zeta} \,\in\, \mathbb{L}^2(\Omega)\,. \tag{2.3}$$

Note that the stress $\boldsymbol{\sigma}$ can be expressed in terms of the pseudostress $\boldsymbol{\rho}$ (see [20, 21]) as

$$\boldsymbol{\sigma} \;\;=\;\; \boldsymbol{\rho} \;+\; \boldsymbol{\rho}^{\mathtt{t}} \;-\; \left\{\frac{\lambda+2\mu}{2\lambda+3\mu}\right\}\,\mathrm{tr}(\boldsymbol{\rho})\,\mathbb{I}\,. \tag{2.4}$$

In addition, other physical quantities of interest such as the strain tensor of small deformations $\mathbf{e}(\mathbf{u})$ and the rotation $\boldsymbol{\gamma} := \frac{1}{2}(\nabla\,\mathbf{u} - (\nabla\,\mathbf{u})^{\mathtt{t}})$ can be computed in terms of the pseudostress $\boldsymbol{\rho}$ by

$$\mathbf{e}(\mathbf{u}) \;=\; \frac{1}{2\mu}\left\{\boldsymbol{\rho} \;+\; \boldsymbol{\rho}^{\mathtt{t}} \;-\; \frac{2(\lambda+\mu)}{2\lambda+3\mu}\,\mathrm{tr}(\boldsymbol{\rho})\,\mathbb{I}\right\} \qquad \text{and} \qquad \boldsymbol{\gamma} \;=\; \frac{1}{4\mu}(\boldsymbol{\rho} \,-\, \boldsymbol{\rho}^{\mathtt{t}})\,.$$

Now, proceeding as in [20, 21], we arrive at the following mixed variational formulation of (2.2): Find $(\boldsymbol{\rho},\mathbf{u}) \in \mathbb{H}\times\mathbf{Q}$ such that

$$\left\{\begin{array}{rcll} a(\boldsymbol{\rho},\boldsymbol{\tau}) \;+\; b(\boldsymbol{\tau},\mathbf{u}) & = & \langle\boldsymbol{\tau}\boldsymbol{n}\,,\mathbf{g}\rangle_{\Gamma} & \forall\;\boldsymbol{\tau}\in\mathbb{H}\,, \\ b(\boldsymbol{\rho},\mathbf{v}) & = & -\displaystyle\int_{\Omega}\mathbf{f}\cdot\mathbf{v} & \forall\;\mathbf{v}\in\mathbf{Q}\,, \end{array}\right. \tag{2.5}$$

where $\mathbb{H} := \mathbb{H}(\mathbf{div};\Omega)$, $\mathbf{Q} := \mathbf{L}^2(\Omega)$, and $a : \mathbb{H}\times\mathbb{H}\to\mathrm{R}$ and $b : \mathbb{H}\times\mathbf{Q}\to\mathrm{R}$ are the bilinear forms

$$a(\boldsymbol{\zeta},\boldsymbol{\tau}) \;:=\; \int_{\Omega}\widetilde{\mathcal{C}}^{-1}\boldsymbol{\zeta} : \boldsymbol{\tau} \;=\; \frac{1}{\mu}\int_{\Omega}\boldsymbol{\zeta} : \boldsymbol{\tau} - \frac{\lambda+\mu}{\mu(2\lambda+3\mu)}\int_{\Omega}\mathrm{tr}(\boldsymbol{\zeta})\,\mathrm{tr}(\boldsymbol{\tau}) \qquad \forall\;\boldsymbol{\zeta},\boldsymbol{\tau}\,\in\,\mathbb{H}\,, \tag{2.6}$$

$$b(\boldsymbol{\tau},\mathbf{v}) \;:=\; \int_{\Omega}\mathbf{v}\cdot\mathbf{div}(\boldsymbol{\tau}) \qquad \forall\;\boldsymbol{\tau}\,\in\,\mathbb{H}\,, \quad \forall\;\mathbf{v}\,\in\,\mathbf{Q}\,, \tag{2.7}$$

and $\langle\cdot,\cdot\rangle_{\Gamma}$ stands from now on for the duality pairing between $\mathbf{H}^{-1/2}(\Gamma)$ and $\mathbf{H}^{1/2}(\Gamma)$. We now define

$$\mathbb{H}_0 := \left\{\boldsymbol{\tau}\in\mathbb{H}(\mathbf{div};\Omega) \;:\; \int_{\Omega}\mathrm{tr}(\boldsymbol{\tau}) = 0\right\}\,,$$

and recall that $\mathbb{H} = \mathbb{H}_0 \oplus \mathrm{R}\,\mathbb{I}$, which means that for any $\boldsymbol{\tau}\in\mathbb{H}$, there exist unique elements $\boldsymbol{\tau}_0\in\mathbb{H}_0$ and $d := \frac{1}{2|\Omega|}\int_{\Omega}\mathrm{tr}(\boldsymbol{\tau})\in\mathrm{R}$, where $|\Omega|$ denotes the measure of Ω, such that $\boldsymbol{\tau} = \boldsymbol{\tau}_0 + d\,\mathbb{I}$. In particular, taking $\boldsymbol{\tau} = \mathbb{I}$ in the first equation of (2.5), we deduce that

$$\int_{\Omega}\mathrm{tr}(\boldsymbol{\rho}) \;=\; (2\lambda+3\mu)\int_{\Gamma}\mathbf{g}\cdot\boldsymbol{n}\,,$$

which yields $\boldsymbol{\rho} = \boldsymbol{\rho}_0 + c\,\mathbb{I}$, with $\boldsymbol{\rho}_0\in\mathbb{H}_0$ and the constant c given explicitly by

$$c \;:=\; \frac{2\lambda+3\mu}{2|\Omega|}\int_{\Gamma}\mathbf{g}\cdot\boldsymbol{n}\,. \tag{2.8}$$

In this way, replacing $\boldsymbol{\rho}$ by the expression $\boldsymbol{\rho}_0 + c\,\mathbb{I}$ in (2.5), and similarly as in [20, 21], using that $\mathbf{div}(\boldsymbol{\rho}) = \mathbf{div}(\boldsymbol{\rho}_0)$ and denoting the remaining unknown $\boldsymbol{\rho}_0\in\mathbb{H}_0$ simply by $\boldsymbol{\rho}$ from now on, we find that the dual-mixed variational formulation (2.5) is equivalent to the following saddle point problem: Find $(\boldsymbol{\rho},\mathbf{u})\in\mathbb{H}_0\times\mathbf{Q}$ such that

$$\left\{\begin{array}{rcll} a(\boldsymbol{\rho},\boldsymbol{\tau}) \;+\; b(\boldsymbol{\tau},\mathbf{u}) & = & \langle\boldsymbol{\tau}\boldsymbol{n}\,,\mathbf{g}\rangle_{\Gamma} & \forall\;\boldsymbol{\tau}\in\mathbb{H}_0\,, \\ b(\boldsymbol{\rho},\mathbf{v}) & = & -\displaystyle\int_{\Omega}\mathbf{f}\cdot\mathbf{v} & \forall\;\mathbf{v}\in\mathbf{Q}\,. \end{array}\right. \tag{2.9}$$

Lemma 2.1. *Problems* (2.5) *and* (2.9) *are equivalent in the following sense:*

i) If $(\boldsymbol{\rho}, \mathbf{u}) \in \mathbb{H} \times \mathbf{Q}$ *is a solution of* (2.5) *and* $\boldsymbol{\rho} = \boldsymbol{\rho}_0 + c\,\mathbb{I}$ *for some* $\boldsymbol{\rho}_0 \in \mathbb{H}_0$ *and* $c \in \mathrm{R}$*, then* $(\boldsymbol{\rho}_0, \mathbf{u}) \in \mathbb{H}_0 \times \mathbf{Q}$ *is a solution of* (2.9)*.*

ii) If $(\boldsymbol{\rho}_0, \mathbf{u}) \in \mathbb{H}_0 \times \mathbf{Q}$ *is a solution of* (2.9) *and* $\boldsymbol{\rho} := \boldsymbol{\rho}_0 + c\,\mathbb{I}$ *with* c *given by* (2.8)*, then* $(\boldsymbol{\rho}, \mathbf{u}) \in \mathbb{H} \times \mathbf{Q}$ *is a solution of* (2.5)*.*

Proof. See [21, Lemma 2.1]. □

Furthermore, according to the new meaning of $\boldsymbol{\rho}$, we deduce from (2.2) and (2.8) that the constitutive equation in (2.2) becomes

$$\widetilde{\mathcal{C}}^{-1}\boldsymbol{\rho} \;+\; \left\{\frac{1}{2|\Omega|}\int_\Gamma \mathbf{g}\cdot\boldsymbol{n}\right\}\mathbb{I} \;=\; \nabla\mathbf{u} \quad \text{in} \quad \Omega\,,$$

whereas the equilibrium equation remains the same, that is

$$\mathbf{div}(\boldsymbol{\rho}) \;=\; -\mathbf{f} \quad \text{in} \quad \Omega\,.$$

In addition, in terms of the $\mathbb{H}_0$-component of the pseudostress, the stress (cf. (2.4)) is now given by

$$\boldsymbol{\sigma} \;=\; \boldsymbol{\rho} \;+\; \boldsymbol{\rho}^{\mathtt{t}} \;-\; \left\{\frac{\lambda+2\mu}{2\lambda+3\mu}\,\mathrm{tr}(\boldsymbol{\rho}) - \frac{\lambda+\mu}{|\Omega|}\int_\Gamma \mathbf{g}\cdot\boldsymbol{n}\right\}\mathbb{I}\,. \tag{2.10}$$

The unique solvability of (2.9) is established as follows.

Theorem 2.1. *Assume that* $\mathbf{f} \in \mathbf{L}^2(\Omega)$ *and* $\mathbf{g} \in \mathbf{H}^{1/2}(\Gamma)$*. Then, there exists a unique solution* $(\boldsymbol{\rho}, \mathbf{u}) \in \mathbb{H}_0 \times \mathbf{Q}$ *to* (2.9)*. In addition, there exists* $C > 0$*, independent of* λ*, such that*

$$\|\boldsymbol{\rho}\|_{\mathbf{div};\Omega} \;+\; \|\mathbf{u}\|_{0,\Omega} \;\leq\; C\left\{\|\mathbf{f}\|_{0,\Omega} \;+\; \|\mathbf{g}\|_{1/2,\Gamma}\right\}.$$

Proof. See [21, Theorem 2.1]. □

3 The mixed virtual element method

In this section we introduce and analyze a mixed virtual element scheme for the equivalent continuous formulation given by (2.9).

3.1 Basic assumptions

Let $\{\mathcal{T}_h\}_{h>0}$ be a family of decompositions of Ω in polygonal elements. For each $K \in \mathcal{T}_h$, we denote its diameter by h_K and define, as usual, $h := \max\{h_K : K \in \mathcal{T}_h\}$. Furthermore, in what follows we assume that there exists a constant $C_{\mathcal{T}} > 0$ such that for each decomposition $\mathcal{T}_h$ and for each $K \in \mathcal{T}_h$, there hold:

a) the ratio between the shortest edge and the diameter h_K of K is bigger than $C_{\mathcal{T}}$, and

b) K is star-shaped with respect to a ball B of radius $C_{\mathcal{T}} h_K$ and center $\mathbf{x}_B \in K$, that is, for each $\mathbf{x}_0 \in B$, all the line segments joining $\mathbf{x}_0$ with any $\mathbf{x} \in K$ are contained in K, or, equivalently, for each $\mathbf{x} \in K$, the closed convex hull of $\{\mathbf{x}\} \cup B$ is contained in K.

As a consequence of the above hypotheses, one can show that each $K \in \mathcal{T}_h$ is simply connected, and that there exists an integer $N_{\mathcal{T}}$ (depending only on $C_{\mathcal{T}}$), such that for each $K \in \mathcal{T}_h$, d_K is bounded above by $N_{\mathcal{T}}$.

3.2 The virtual element spaces

Given an integer $\ell \geq 0$, we let $\mathrm{P}_\ell(K)$ be the space of polynomials defined on K of total degree at most ℓ. Then, for each integer $k \geq 0$ and for each $K \in \mathcal{T}_h$, we follow [6, 7] (see also [14] and [15]) and consider the following local virtual element subspace of order k

$$\begin{aligned}\mathbb{H}_h^K \ := \ \Big\{ \boldsymbol{\tau} \in \mathbb{H}(\mathbf{div}; K) \cap \mathbb{H}(\mathbf{rot}; K) \ : \quad \boldsymbol{\tau}\boldsymbol{n}|_e \in \mathbf{P}_k(e) \quad \forall \text{ edge } e \in \partial K \, , \\ \mathbf{div}(\boldsymbol{\tau}) \in \mathbf{P}_k(K) \, , \quad \text{and} \quad \mathbf{rot}(\boldsymbol{\tau}) \in \mathbf{P}_{k-1}(K) \Big\} \, ,\end{aligned} \tag{3.1}$$

where $\mathbf{P}_{-1}(K) := \{\mathbf{0}\}$, and

$$\mathbf{rot}(\boldsymbol{\tau}) \ := \ \begin{pmatrix} \partial_{x_1}\tau_{12} - \partial_{x_2}\tau_{11} \\ \partial_{x_1}\tau_{22} - \partial_{x_2}\tau_{21} \end{pmatrix} \qquad \forall \ \boldsymbol{\tau} \in \mathbb{H} \, .$$

We recall here that the virtual subspace $\mathbb{H}_h^K$ was first introduced in [7] and recently utilized in [14] and [15] for a pseudostress-based formulation of the linear Brinkman problem, and for a class of nonlinear Stokes models arising in quasi-Newtonian fluids, respectively.

Next, the corresponding global virtual element subspaces of $\mathbb{H}_0$ and $\mathbf{Q}$, are given, respectively, by

$$\mathbb{H}_{0,h} \ := \ \Big\{ \boldsymbol{\tau} \in \mathbb{H}_0 \ : \quad \boldsymbol{\tau}|_K \in \mathbb{H}_h^K \quad \forall \ K \in \mathcal{T}_h \Big\} \, , \tag{3.2}$$

and

$$\mathbf{Q}_h \ := \ \Big\{ \mathbf{v} \in \mathbf{Q} \ : \quad \mathbf{v}|_K \in \mathbf{P}_k(K) \quad \forall \ K \in \mathcal{T}_h \Big\} \, . \tag{3.3}$$

Then, the Galerkin scheme associated with (2.9) reads: Find $(\boldsymbol{\rho}, \mathbf{u}) \in \mathbb{H}_{0,h} \times \mathbf{Q}_h$ such that

$$\left\{ \begin{array}{rcll} a(\boldsymbol{\rho}_h, \boldsymbol{\tau}_h) \ + \ b(\boldsymbol{\tau}_h, \mathbf{u}_h) & = & \langle \boldsymbol{\tau}_h \boldsymbol{n} \, , \mathbf{g} \rangle_\Gamma & \forall \ \boldsymbol{\tau}_h \in \mathbb{H}_{0,h} \, , \\ b(\boldsymbol{\rho}_h, \mathbf{v}_h) & = & - \displaystyle\int_\Omega \mathbf{f} \cdot \mathbf{v}_h & \forall \ \mathbf{v}_h \in \mathbf{Q}_h \, . \end{array} \right. \tag{3.4}$$

Unfortunately, and similarly as in [11, 13, 14, 15], we will observe in the next section that $a(\boldsymbol{\rho}_h, \boldsymbol{\tau}_h)$ cannot be computed explicitly when $\boldsymbol{\rho}_h, \boldsymbol{\tau}_h$ belong to $\mathbb{H}_{0,h}$, and hence a suitable approximation of this bilinear form, namely $a_h(\cdot, \cdot)$, is required in order to redefine (3.4).

3.3 The discrete bilinear forms

In this section we define computable discrete versions $a_h : \mathbb{H}_{0,h} \times \mathbb{H}_{0,h} \to \mathrm{R}$ and $b_h : \mathbb{H}_{0,h} \times \mathbf{Q}_h \to \mathrm{R}$ of the bilinear forms $a(\cdot, \cdot)$ and $b(\cdot, \cdot)$. To this end, we proceed as in [13, Section 4] and observe first that given $(\boldsymbol{\tau}_h, \mathbf{v}_h) \in \mathbb{H}_{0,h} \times \mathbf{Q}_h$, the expression

$$b(\boldsymbol{\tau}_h, \mathbf{v}_h) \ := \ \int_\Omega \mathbf{v}_h \cdot \mathbf{div}(\boldsymbol{\tau}_h) \ = \ \sum_{K \in \mathcal{T}_h} \int_K \mathbf{v}_h \cdot \mathbf{div}(\boldsymbol{\tau}_h) \, ,$$

is explicitly calculable since according to the definitions of $\mathbb{H}_{0,h}$ and $\mathbf{Q}_h$ (cf. (3.2) and (3.3)), there hold $\mathbf{v}_h|_K \in \mathbf{P}_k(K)$ and $\mathbf{div}(\boldsymbol{\tau}_h)|_K \in \mathbf{P}_k(K)$ on each element K, and hence we just set $b_h := b$. On the contrary, given $\boldsymbol{\zeta}_h, \boldsymbol{\tau}_h \in \mathbb{H}_{0,h}$, the expression

$$a(\boldsymbol{\zeta}_h, \boldsymbol{\tau}_h) \ := \ \int_\Omega \widetilde{\mathcal{C}}^{-1} \boldsymbol{\zeta}_h : \boldsymbol{\tau}_h \ = \ \frac{1}{\mu} \int_\Omega \boldsymbol{\zeta}_h : \boldsymbol{\tau}_h - \frac{\lambda + \mu}{\mu(2\lambda + 3\mu)} \int_\Omega \mathrm{tr}(\boldsymbol{\zeta}_h) \, \mathrm{tr}(\boldsymbol{\tau}_h)$$

is not explicitly calculable since in general $\boldsymbol{\zeta}_h$ and $\boldsymbol{\tau}_h$ are not known on each $K \in \mathcal{T}_h$. In order to overcome this difficulty, we now introduce a suitable space on which the elements of $\mathbb{H}_{0,h}$ will be projected later on, so that the bilinear form $a(\cdot,\cdot)$ is explicitly computable for these projections. Indeed, we let $\boldsymbol{\mathcal{P}}_k^K : \mathbb{L}^2(K) \to \mathbb{P}_k(K)$ be the $\mathbb{L}^2(K)$-orthogonal projector. That is, given $\boldsymbol{\zeta} \in \mathbb{L}^2(K)$, $\boldsymbol{\mathcal{P}}_k^K(\boldsymbol{\zeta})$ is characterized by

$$\int_K \boldsymbol{\mathcal{P}}_k^K(\boldsymbol{\zeta}) : \boldsymbol{\tau} \;=\; \int_K \boldsymbol{\zeta} : \boldsymbol{\tau} \qquad \forall\, \boldsymbol{\tau} \in \mathbb{P}_k(K) \tag{3.5}$$

which, according to [7, Section 3.2] (see also [14, Section 3.1.1]), is explicitly calculable, even when $\boldsymbol{\zeta} \in \mathbb{H}_h^K$. In addition, it is straightforward to check from (3.5) with $\boldsymbol{\tau} = \boldsymbol{\mathcal{P}}_k^K(\boldsymbol{\zeta})$ that

$$\|\boldsymbol{\mathcal{P}}_k^K(\boldsymbol{\zeta})\|_{0,K} \;\leq\; \|\boldsymbol{\zeta}\|_{0,K} \qquad \forall\, \boldsymbol{\zeta} \in \mathbb{L}^2(K)\,. \tag{3.6}$$

Furthermore, the operator $\boldsymbol{\mathcal{P}}_k^K$ satisfies the following approximation property (see, e.g. [7, eq. (22)] or [13, Lemma 3.4]): for each $\boldsymbol{\zeta} \in \mathbb{H}^r(K)$, with $0 \leq r \leq k+1$, there holds

$$\|\boldsymbol{\zeta} - \boldsymbol{\mathcal{P}}_k^K(\boldsymbol{\zeta})\|_{0,K} \;\leq\; C\, h_K^r\, |\boldsymbol{\zeta}|_{r,K} \quad \forall\, K \in \mathcal{T}_h\,. \tag{3.7}$$

Now, for each $K \in \mathcal{T}_h$, we let $a^K : \mathbb{L}^2(K) \times \mathbb{L}^2(K) \to \mathrm{R}$ be the local bilinear form defined by

$$a^K(\boldsymbol{\zeta},\boldsymbol{\tau}) \;:=\; \int_K \widetilde{\mathcal{C}}^{-1}\boldsymbol{\zeta} : \boldsymbol{\tau} \qquad \forall\, \boldsymbol{\zeta},\boldsymbol{\tau} \in \mathbb{L}^2(K)\,, \tag{3.8}$$

whence a (cf. (2.6)) can be rewritten as

$$a(\boldsymbol{\zeta},\boldsymbol{\tau}) \;:=\; \sum_{K\in\mathcal{T}_h} a^K(\boldsymbol{\zeta}|_K,\boldsymbol{\tau}|_K) \qquad \forall\, \boldsymbol{\zeta},\, \boldsymbol{\tau} \in \mathbb{L}^2(\Omega)\,. \tag{3.9}$$

Then, applying the Cauchy-Schwarz inequality and using that $\frac{\lambda+\mu}{2\lambda+3\mu} < \frac{1}{2}$, we find that

$$\begin{aligned} |a^K(\boldsymbol{\zeta},\,\boldsymbol{\tau})| \;&=\; \frac{1}{\mu}\left|\int_K \boldsymbol{\zeta} : \boldsymbol{\tau} \;-\; \frac{\lambda+\mu}{2\lambda+3\mu}\int_K \mathrm{tr}(\boldsymbol{\zeta})\,\mathrm{tr}(\boldsymbol{\tau})\right| \\ &\leq\; \frac{1}{\mu}\,\|\boldsymbol{\zeta}\|_{0,K}\|\boldsymbol{\tau}\|_{0,K} \;+\; \frac{1}{2\mu}\,\|\mathrm{tr}(\boldsymbol{\zeta})\|_{0,K}\|\mathrm{tr}(\boldsymbol{\tau})\|_{0,K} \\ &\leq\; \frac{1}{\mu}\,\|\boldsymbol{\zeta}\|_{0,K}\|\boldsymbol{\tau}\|_{0,K} \;+\; \frac{1}{\mu}\,\|\boldsymbol{\zeta}\|_{0,K}\|\boldsymbol{\tau}\|_{0,K} \;=\; \frac{2}{\mu}\,\|\boldsymbol{\zeta}\|_{0,K}\|\boldsymbol{\tau}\|_{0,K} \end{aligned} \tag{3.10}$$

for all $\boldsymbol{\zeta},\boldsymbol{\tau} \in \mathbb{L}^2(K)$. Moreover, replacing $\boldsymbol{\zeta} = \boldsymbol{\zeta}^{\mathrm{d}} + \frac{1}{2}\,\mathrm{tr}(\boldsymbol{\zeta})\,\mathbb{I}$ in (3.8), and using that $\boldsymbol{\zeta}^{\mathrm{d}} : \boldsymbol{\tau} = \boldsymbol{\zeta}^{\mathrm{d}} : \boldsymbol{\tau}^{\mathrm{d}}$, and $\mathrm{tr}(\boldsymbol{\zeta}^{\mathrm{d}}) = 0$ for all $\boldsymbol{\zeta} \in \mathbb{L}^2(K)$, we arrive at the following equivalent expression for a^K:

$$a^K(\boldsymbol{\zeta},\boldsymbol{\tau}) \;=\; \frac{1}{\mu}\int_K \boldsymbol{\zeta}^{\mathrm{d}} : \boldsymbol{\tau}^{\mathrm{d}} \;+\; \frac{1}{2(2\lambda+3\mu)}\int_K \mathrm{tr}(\boldsymbol{\zeta})\,\mathrm{tr}(\boldsymbol{\tau}) \qquad \forall\, \boldsymbol{\zeta},\boldsymbol{\tau} \in \mathbb{L}^2(K)\,,$$

In particular,

$$a^K(\boldsymbol{\zeta},\boldsymbol{\zeta}) \;\geq\; \frac{1}{\mu}\,\|\boldsymbol{\zeta}^{\mathrm{d}}\|_{0,K}^2 \qquad \forall\, \boldsymbol{\zeta} \in \mathbb{L}^2(K)\,, \quad \forall\, K \in \mathcal{T}_h\,. \tag{3.11}$$

In turn, we let $a_h^K : \mathbb{H}_h^K \times \mathbb{H}_h^K \to \mathrm{R}$ be the local discrete bilinear form given for all $\boldsymbol{\zeta},\boldsymbol{\tau} \in \mathbb{H}_h^K$ by

$$a_h^K(\boldsymbol{\zeta},\boldsymbol{\tau}) \;:=\; a^K(\boldsymbol{\mathcal{P}}_k^K(\boldsymbol{\zeta}),\,\boldsymbol{\mathcal{P}}_k^K(\boldsymbol{\tau})) \;+\; \mathcal{S}^K(\boldsymbol{\zeta}-\boldsymbol{\mathcal{P}}_k^K(\boldsymbol{\zeta}),\,\boldsymbol{\tau}-\boldsymbol{\mathcal{P}}_k^K(\boldsymbol{\tau}))\,, \tag{3.12}$$

where $\mathcal{S}^K : \mathbb{H}_h^K \times \mathbb{H}_h^K \to \mathrm{R}$ is the bilinear form associated to the n_k^K local degrees of freedom of $\mathbb{H}_h^K$ (see, e.g, [14, Section 3.2]). More precisely,

$$\mathcal{S}^K(\boldsymbol{\zeta},\,\boldsymbol{\tau}) \;:=\; \sum_{i=1}^{n_k^K} m_{i,K}(\boldsymbol{\zeta})\, m_{i,K}(\boldsymbol{\tau}) \qquad \forall\, \boldsymbol{\zeta},\boldsymbol{\tau} \in \mathbb{H}_h^K\,, \tag{3.13}$$

where the set $\{m_{i,K}(\boldsymbol{\tau})\}_{i=1}^{n_k^K}$ corresponds to all the K-moments of $\boldsymbol{\tau} \in \mathbb{H}_h^K$ (cf. (3.1)), given by (see, e.g, [14, Section 3.2])

$$\begin{aligned}
&\int_e \boldsymbol{\tau}\boldsymbol{n}\cdot\mathbf{q} \qquad \forall\, \mathbf{q} \in \mathbf{P}_k(e)\,, \quad \forall \text{ edge } e \in \partial K\,,\\
&\int_K \boldsymbol{\tau} : \nabla\mathbf{q} \qquad \forall\, \mathbf{q} \in \mathbf{P}_k(K) \setminus \{(1,0)^{\mathtt{t}},\,(0,1)^{\mathtt{t}}\}\,,\\
&\int_K \boldsymbol{\tau} : \boldsymbol{\xi} \qquad \forall\, \boldsymbol{\xi} \in (\nabla\mathbf{P}_{k+1}(K))^{\perp} \cap \mathbb{P}_k(K)\,.
\end{aligned}$$

In addition, as in [11, eq. (5.8)], we assume that there exist $c_0, c_1 > 0$, independent of λ and K, such that

$$c_0\,\|\boldsymbol{\zeta}\|_{0,K}^2 \;\le\; \mathcal{S}^K(\boldsymbol{\zeta},\boldsymbol{\zeta}) \;\le\; c_1\,\|\boldsymbol{\zeta}\|_{0,K}^2 \qquad \forall\, \boldsymbol{\zeta} \in \mathbb{H}_h^K, \quad \forall\, K \in \mathcal{T}_h\,. \tag{3.14}$$

The following result is a consequence of the properties from the projector $\boldsymbol{\mathcal{P}}_k^K$ and (3.14).

Lemma 3.1. *For each $K \in \mathcal{T}_h$, there holds*

$$a_h^K(\boldsymbol{\zeta},\boldsymbol{\tau}) \;=\; a^K(\boldsymbol{\zeta},\boldsymbol{\tau}) \qquad \forall\, \boldsymbol{\zeta} \in \mathbb{P}_k(K)\,, \quad \forall\, \boldsymbol{\tau} \in \mathbb{H}_h^K\,, \tag{3.15}$$

and there exist positive constants α_1, α_2, independent of h, λ and K, such that

$$|a_h^K(\boldsymbol{\zeta},\boldsymbol{\tau})| \;\le\; \alpha_1\Big\{\|\boldsymbol{\zeta}\|_{0,K}\|\boldsymbol{\tau}\|_{0,K} \,+\, \|\boldsymbol{\zeta}-\boldsymbol{\mathcal{P}}_k^K(\boldsymbol{\zeta})\|_{0,K}\|\boldsymbol{\tau}-\boldsymbol{\mathcal{P}}_k^K(\boldsymbol{\tau})\|_{0,K}\Big\} \quad \forall\, \boldsymbol{\zeta},\boldsymbol{\tau} \in \mathbb{H}_h^K\,, \tag{3.16}$$

and

$$\alpha_2\,\|\boldsymbol{\zeta}^{\mathrm{d}}\|_{0,K}^2 \;\le\; a_h^K(\boldsymbol{\zeta},\boldsymbol{\zeta}) \quad \forall\, \boldsymbol{\zeta} \in \mathbb{H}_h^K\,. \tag{3.17}$$

Proof. We adapt the proof of [13, Lemma 4.6]. Indeed, we first note that given $\boldsymbol{\zeta} \in \mathbb{P}_k(K)$, it holds $\boldsymbol{\mathcal{P}}_k^K(\boldsymbol{\zeta}) = \boldsymbol{\zeta}$. Hence, using the definition of a^K (cf. (3.8)), the fact that $\widetilde{\mathcal{C}}^{-1}\boldsymbol{\zeta} \in \mathbb{P}_k(K)$ (cf. (2.3)) and (3.5), we deduce, starting from (3.12), that given $\boldsymbol{\tau} \in \mathbb{H}_h^K$ there holds

$$\begin{aligned}
a_h^K(\boldsymbol{\zeta},\boldsymbol{\tau}) \;&=\; a^K(\boldsymbol{\zeta},\boldsymbol{\mathcal{P}}_k^K(\boldsymbol{\tau})) \;=\; \int_K \widetilde{\mathcal{C}}^{-1}\boldsymbol{\zeta} : \boldsymbol{\mathcal{P}}_k^K(\boldsymbol{\tau}) \;=\; \int_K \boldsymbol{\mathcal{P}}_k^K(\boldsymbol{\tau}) : \widetilde{\mathcal{C}}^{-1}\boldsymbol{\zeta}\\
&=\; \int_K \boldsymbol{\tau} : \widetilde{\mathcal{C}}^{-1}\boldsymbol{\zeta} \;=\; \int_K \widetilde{\mathcal{C}}^{-1}\boldsymbol{\zeta} : \boldsymbol{\tau} \;=\; a^K(\boldsymbol{\zeta},\boldsymbol{\tau})\,,
\end{aligned}$$

which proves (3.15). Next, for the boundedness of a_h^K we apply the Cauchy-Schwarz inequality, the estimate (3.10), and the upper bound in (3.14), to obtain

$$\begin{aligned}
|a_h^K(\boldsymbol{\zeta},\boldsymbol{\tau})| \;&\le\; |a^K(\,\boldsymbol{\mathcal{P}}_k^K(\boldsymbol{\zeta}),\,\boldsymbol{\mathcal{P}}_k^K(\boldsymbol{\tau})\,)|\\
&\quad+\; \big\{\mathcal{S}^K(\boldsymbol{\zeta}-\boldsymbol{\mathcal{P}}_k^K(\boldsymbol{\zeta}),\boldsymbol{\zeta}-\boldsymbol{\mathcal{P}}_k^K(\boldsymbol{\zeta}))\big\}^{1/2}\,\big\{\mathcal{S}^K(\boldsymbol{\tau}-\boldsymbol{\mathcal{P}}_k^K(\boldsymbol{\tau}),\boldsymbol{\tau}-\boldsymbol{\mathcal{P}}_k^K(\boldsymbol{\tau}))\big\}^{1/2}\\
&\le\; \frac{2}{\mu}\,\|\boldsymbol{\mathcal{P}}_k^K(\boldsymbol{\zeta})\|_{0,K}\|\boldsymbol{\mathcal{P}}_k^K(\boldsymbol{\tau})\|_{0,K} \,+\, c_1\|\boldsymbol{\zeta}-\boldsymbol{\mathcal{P}}_k^K(\boldsymbol{\zeta})\|_{0,K}\|\boldsymbol{\tau}-\boldsymbol{\mathcal{P}}_k^K(\boldsymbol{\tau})\|_{0,K} \quad \forall\, \boldsymbol{\zeta},\boldsymbol{\tau} \in \mathbb{H}_h^K\,,
\end{aligned}$$

which, together with (3.6), imply (3.16) with $\alpha_1 := \max\{\frac{2}{\mu}, c_1\}$. Finally, concerning (3.17), we apply the lower bound in (3.14) and (3.11), to obtain

$$\begin{aligned}\|\boldsymbol{\zeta}^{\mathrm{d}}\|_{0,K}^2 &\leq 2\left\{\|(\boldsymbol{\mathcal{P}}_k^K(\boldsymbol{\zeta}))^{\mathrm{d}}\|_{0,K}^2 \;+\; \|(\boldsymbol{\zeta}-\boldsymbol{\mathcal{P}}_k^K(\boldsymbol{\zeta}))^{\mathrm{d}}\|_{0,K}^2\right\}\\ &\leq 2\mu\left(\frac{1}{\mu}\,\|(\boldsymbol{\mathcal{P}}_k^K(\boldsymbol{\zeta}))^{\mathrm{d}}\|_{0,K}^2\right) \;+\; \frac{2}{c_0}\left(c_0\|\boldsymbol{\zeta}-\boldsymbol{\mathcal{P}}_k^K(\boldsymbol{\zeta})\|_{0,K}^2\right)\\ &\leq 2\mu\, a^K(\boldsymbol{\mathcal{P}}_k^K(\boldsymbol{\zeta}),\boldsymbol{\mathcal{P}}_k^K(\boldsymbol{\zeta})) \;+\; \frac{2}{c_0}\,\mathcal{S}^K(\boldsymbol{\zeta}-\boldsymbol{\mathcal{P}}_k^K(\boldsymbol{\zeta}),\boldsymbol{\zeta}-\boldsymbol{\mathcal{P}}_k^K(\boldsymbol{\zeta})) \quad \forall\,\boldsymbol{\zeta}\in\mathbb{H}_h^K\,,\end{aligned}$$

which yields (3.17) with $\alpha_2 := \max\{2\mu, \frac{2}{c_0}\}^{-1}$, and completes the proof. □

We end this section by defining, as suggested by (3.9) and (3.12), the global discrete bilinear form $a_h : \mathbb{H}_{0,h}\times\mathbb{H}_{0,h}\to\mathrm{R}$ by

$$a_h(\boldsymbol{\zeta},\boldsymbol{\tau}) \;:=\; \sum_{K\in\mathcal{T}_h} a_h^K(\boldsymbol{\zeta},\boldsymbol{\tau}) \qquad \forall\,\boldsymbol{\zeta},\boldsymbol{\tau}\in\mathbb{H}_{0,h}\,. \tag{3.18}$$

3.4 The mixed virtual element scheme

According to the analysis from the foregoing section, we reformulate the Galerkin scheme (3.4) associated with (2.9) as: Find $(\boldsymbol{\rho},\mathbf{u})\in\mathbb{H}_{0,h}\times\mathbf{Q}_h$ such that

$$\left\{\begin{array}{rcll} a_h(\boldsymbol{\rho}_h,\boldsymbol{\tau}_h) \;+\; b(\boldsymbol{\tau}_h,\mathbf{u}_h) &=& \langle\boldsymbol{\tau}_h\boldsymbol{n}\,,\mathbf{g}\rangle_\Gamma & \forall\,\boldsymbol{\tau}_h\in\mathbb{H}_{0,h}\,,\\ b(\boldsymbol{\rho}_h,\mathbf{v}_h) &=& -\displaystyle\int_\Omega \mathbf{f}\cdot\mathbf{v}_h & \forall\,\mathbf{v}_h\in\mathbf{Q}_h\,. \end{array}\right. \tag{3.19}$$

In what follows we establish the well-posedness of (3.19). We begin the analysis by proving that $a_h(\cdot,\cdot)$ is elliptic in the discrete kernel of $b(\cdot,\cdot)$.

Lemma 3.2. *Let $\mathbb{V}_h := \{\boldsymbol{\zeta}_h\in\mathbb{H}_{0,h} \,:\, b(\boldsymbol{\zeta}_h,\mathbf{v}_h)=0 \;\;\forall\,\mathbf{v}_h\in\mathbf{Q}_h\}$. Then, there exists $\alpha>0$, independent of h and λ, such that*

$$a_h(\boldsymbol{\zeta}_h,\boldsymbol{\zeta}_h) \;\geq\; \alpha\,\|\boldsymbol{\zeta}_h\|_{\mathbf{div};\Omega}^2 \qquad \forall\,\boldsymbol{\zeta}_h\in\mathbb{V}_h\,.$$

Proof. It follows exactly as in [13, Lemma 5.2]. □

The following lemma provides the discrete inf-sup condition for $b(\cdot,\cdot)$.

Lemma 3.3. *Let $\mathbb{H}_{0,h}$ and $\mathbf{Q}_h$ be the virtual subspaces given by* (3.2) *and* (3.3)*. Then, there exists $\beta>0$, independent of h and λ, such that*

$$\sup_{\substack{\boldsymbol{\tau}_h\in\mathbb{H}_{0,h}\\ \boldsymbol{\tau}_h\neq\mathbf{0}}} \frac{b(\boldsymbol{\tau}_h,\,\mathbf{v}_h)}{\|\boldsymbol{\tau}_h\|_{\mathbf{div};\Omega}} \;\geq\; \beta\,\|\mathbf{v}_h\|_{0,\Omega} \qquad \forall\,\mathbf{v}_h\in\mathbf{Q}_h\,. \tag{3.20}$$

Proof. See [13, Lemma 5.3]. □

The unique solvability and stability of the actual Galerkin scheme (3.19) is established next.

Theorem 3.1. *There exists a unique $(\boldsymbol{\rho}_h,\mathbf{u}_h)\in\mathbb{H}_{0,h}\times\mathbf{Q}_h$ solution of* (3.19)*, and there exists a positive constant C, independent of h and λ, such that*

$$\|\boldsymbol{\rho}_h\|_{\mathbf{div};\Omega} \;+\; \|\mathbf{u}_h\|_{0,\Omega} \;\leq\; C\left\{\|\mathbf{f}\|_{0,\Omega} \;+\; \|\mathbf{g}\|_{1/2,\Gamma}\right\}.$$

Proof. The boundedness of $a_h : \mathbb{H}_{0,h} \times \mathbb{H}_{0,h} \to \mathrm{R}$ with respect to the norm $\|\cdot\|_{\mathbf{div};\Omega}$ of $\mathbb{H}(\mathbf{div};\Omega)$ follows directly from (3.18), (3.16), and (3.6). In turn, it is quite clear that $b : \mathbb{H}_{0,h} \times \mathbf{Q}_h \to \mathrm{R}$ is also bounded. Hence, thanks to Lemmas 3.2 and 3.3, a straightforward application of the Babuška-Brezzi theory completes the proof. □

3.5 The a priori error analysis

We now aim to derive the corresponding *a priori* error estimates for (3.19) and (2.9). For this purpose, we need the approximation properties of the virtual element subspaces involved. Thus, letting

$$\mathbb{H}_h^1(\Omega) := \big\{ \boldsymbol{\tau} \in \mathbb{H}(\mathbf{div};\Omega) \ : \quad \boldsymbol{\tau}|_K \in \mathbb{H}^1(K) \quad \forall\, K \in \mathcal{T}_h \big\}\,,$$

we now introduce the interpolation operator $\Pi_k^h : \mathbb{H}_h^1(\Omega) \to \mathbb{H}_{0,h}$ (see [7, 14]), which, given $\boldsymbol{\tau} \in \mathbb{H}_h^1(\Omega)$, is characterized by the following identities:

$$\begin{aligned}
0 &= \int_e \big(\boldsymbol{\tau} - \Pi_k^h(\boldsymbol{\tau})\big)\boldsymbol{n} \cdot \mathbf{q} \quad \forall\, \mathbf{q} \in \mathbf{P}_k(e)\,, && \forall \text{ edge } e \in \mathcal{T}_h\,,\\
0 &= \int_K \big(\boldsymbol{\tau} - \Pi_k^h(\boldsymbol{\tau})\big) : \nabla \mathbf{q} \quad \forall\, \mathbf{q} \in \mathbf{P}_k(K) \setminus \{(1,0)^{\mathtt{t}}, (0,1)^{\mathtt{t}}\}\,, && \forall\, K \in \mathcal{T}_h\,,\\
0 &= \int_K \big(\boldsymbol{\tau} - \Pi_k^h(\boldsymbol{\tau})\big) : \boldsymbol{\xi} \quad \forall\, \boldsymbol{\xi} \in (\nabla \mathbf{P}_{k+1}(K))^{\perp} \cap \mathbb{P}_k(K)\,, && \forall\, K \in \mathcal{T}_h\,.
\end{aligned}$$

Furthermore, we can show (see, e.g, [14, eq. (3.8)]) by using the above identities that

$$\mathbf{div}(\Pi_k^h(\boldsymbol{\tau})) \ = \ \mathcal{P}_k^h(\mathbf{div}(\boldsymbol{\tau}))\,, \tag{3.21}$$

where $\mathcal{P}_k^h : \mathbf{L}^2(\Omega) \to \mathbf{Q}_h$ is the $\mathbf{L}^2(\Omega)$-orthogonal projector. Also, note that $\mathcal{P}_k^h(\mathbf{v})|_K = \mathcal{P}_k^K(\mathbf{v}|_K)$ for each $K \in \mathcal{T}_h$ and for all $\mathbf{v} \in \mathbf{L}^2(\Omega)$, where $\mathcal{P}_k^K : \mathbf{L}^2(K) \to \mathbf{P}_k(K)$ is the local orthogonal projector. Hence, for each $\mathbf{v} \in \mathbf{H}^r(\Omega)$, with $0 \le r \le k+1$, there holds (see, e.g. [7, eq. (22)] or [13, Lemma 3.4])

$$\|\mathbf{v} - \mathcal{P}_k^h(\mathbf{v})\|_{0,K} \ = \ \|\mathbf{v} - \mathcal{P}_k^K(\mathbf{v})\|_{0,K} \ \le \ C\, h_K^r\, |\mathbf{v}|_{r,K} \quad \forall\, K \in \mathcal{T}_h\,. \tag{3.22}$$

In addition, the operator Π_k^h satisfies the following approximation properties (see [7, eq. (28)]): for each $\boldsymbol{\tau} \in \mathbb{H}^r(K)$, with $1 \le r \le k+1$, there holds

$$\|\boldsymbol{\tau} - \Pi_k^h(\boldsymbol{\tau})\|_{0,K} \ \le \ C\, h_K^r\, |\boldsymbol{\tau}|_{r,K} \qquad \forall\, K \in \mathcal{T}_h\,, \tag{3.23}$$

and for each $\boldsymbol{\tau} \in \mathbb{H}_h^1(\Omega)$ such that $\mathbf{div}(\boldsymbol{\tau}) \in \mathbf{H}^r(\Omega)$, with $0 \le r \le k+1$, there holds

$$\|\mathbf{div}(\boldsymbol{\tau} - \Pi_k^h(\boldsymbol{\tau}))\|_{0,K} \ \le \ C\, h_K^r\, |\mathbf{div}(\boldsymbol{\tau})|_{r,K} \qquad \forall\, K \in \mathcal{T}_h\,. \tag{3.24}$$

In particular, note that (3.24) follows easily from (3.21) and (3.22).

Next, recalling the $\mathbb{L}^2(K)$-orthogonal projector $\boldsymbol{\mathcal{P}}_k^K : \mathbb{L}^2(K) \to \mathbb{P}_k(K)$ defined by (3.5), we denote by $\boldsymbol{\mathcal{P}}_k^h$ its global counterpart, that is, given $\boldsymbol{\zeta} \in \mathbb{L}^2(\Omega)$, we let

$$\boldsymbol{\mathcal{P}}_k^h(\boldsymbol{\zeta})|_K \ := \ \boldsymbol{\mathcal{P}}_k^K(\boldsymbol{\zeta}|_K) \qquad \forall\, K \in \mathcal{T}_h\,.$$

Then, we have the following main result.

Theorem 3.2. *Let $(\boldsymbol{\rho}, \mathbf{u}) \in \mathbb{H}_0 \times \mathbf{Q}$ and $(\boldsymbol{\rho}_h, \mathbf{u}_h) \in \mathbb{H}_{0,h} \times \mathbf{Q}_h$ be the unique solutions of the continuous and discrete schemes* (2.9) *and* (3.19)*, respectively, and assume that $\boldsymbol{\rho} \in \mathbb{H}_h^1(\Omega)$. Then, there exist positive constants C_1, C_2, independent of h and λ, such that*

$$\|\boldsymbol{\rho} - \boldsymbol{\rho}_h\|_{0,\Omega} \ \le \ C_1 \Big\{ \|\boldsymbol{\rho} - \Pi_k^h(\boldsymbol{\rho})\|_{0,\Omega} \ + \ \|\boldsymbol{\rho} - \boldsymbol{\mathcal{P}}_k^h(\boldsymbol{\rho})\|_{0,\Omega} \Big\}\,, \tag{3.25}$$

$$\|\mathbf{div}(\boldsymbol{\rho}-\boldsymbol{\rho}_h)\|_{0,\Omega} \;=\; \|\mathbf{div}(\boldsymbol{\rho}-\Pi_k^h(\boldsymbol{\rho}))\|_{0,\Omega}\,, \tag{3.26}$$

and

$$\|\mathbf{u}-\mathbf{u}_h\|_{0,\Omega} \;\leq\; C_2\Big\{\|\boldsymbol{\rho}-\Pi_k^h(\boldsymbol{\rho})\|_{0,\Omega} \;+\; \|\boldsymbol{\rho}-\boldsymbol{\mathcal{P}}_k^h(\boldsymbol{\rho})\|_{0,\Omega} \;+\; \|\mathbf{u}-\mathcal{P}_k^h(\mathbf{u})\|_{0,\Omega}\Big\}\,. \tag{3.27}$$

Proof. We adapt the proof of [13, Theorem 5.2] (see also [14, Theorem 5.2]). Indeed, first note from

$$\|\boldsymbol{\rho}-\boldsymbol{\rho}_h\|_{0,\Omega} \;\leq\; \|\boldsymbol{\rho}-\Pi_k^h(\boldsymbol{\rho})\|_{0,\Omega} \;+\; \|\boldsymbol{\delta}_h\|_{0,\Omega}\,, \tag{3.28}$$

that we only need to estimate $\boldsymbol{\delta}_h := \Pi_k^h(\boldsymbol{\rho})-\boldsymbol{\rho}_h \in \mathbb{H}_{0,h}$. To this end, observe from (3.21) and the second equation of (3.19) that $\mathbf{div}(\Pi_k^h(\boldsymbol{\rho})) = \mathcal{P}_k^h(\mathbf{div}(\boldsymbol{\rho})) = \mathcal{P}_k^h(-\mathbf{f}) = \mathbf{div}(\boldsymbol{\rho}_h)$, which establishes that $\boldsymbol{\delta}_h \in \mathbb{V}_h$ (cf. Lemma 3.2) and gives (3.26). Next, applying Lemma 3.2, adding and subtracting $\boldsymbol{\mathcal{P}}_k^h(\boldsymbol{\rho})$, using the first equations of (3.19) and (2.9), and employing (3.15), we find that

$$\begin{aligned}
\alpha\,\|\boldsymbol{\delta}_h\|^2_{\mathbf{div};\Omega} \;\leq\; a_h(\boldsymbol{\delta}_h,\boldsymbol{\delta}_h) \;&=\; a_h(\Pi_k^h(\boldsymbol{\rho}),\boldsymbol{\delta}_h) \;-\; a_h(\boldsymbol{\rho}_h,\boldsymbol{\delta}_h)\\
&=\; a_h(\Pi_k^h(\boldsymbol{\rho})-\boldsymbol{\mathcal{P}}_k^h(\boldsymbol{\rho}),\boldsymbol{\delta}_h) \;+\; a_h(\boldsymbol{\mathcal{P}}_k^h(\boldsymbol{\rho}),\boldsymbol{\delta}_h) \;-\; \langle\boldsymbol{\delta}_h\boldsymbol{n},\mathbf{g}\rangle_\Gamma\\
&=\; a_h(\Pi_k^h(\boldsymbol{\rho})-\boldsymbol{\mathcal{P}}_k^h(\boldsymbol{\rho}),\boldsymbol{\delta}_h) \;+\; a_h(\boldsymbol{\mathcal{P}}_k^h(\boldsymbol{\rho}),\boldsymbol{\delta}_h) \;-\; a(\boldsymbol{\rho},\boldsymbol{\delta}_h)\\
&=\; \sum_{K\in\mathcal{T}_h}\Big\{a_h^K(\Pi_k^h(\boldsymbol{\rho})-\boldsymbol{\mathcal{P}}_k^K(\boldsymbol{\rho}),\boldsymbol{\delta}_h) \;-\; a^K(\boldsymbol{\rho}-\boldsymbol{\mathcal{P}}_k^K(\boldsymbol{\rho}),\boldsymbol{\delta}_h)\Big\}\,.
\end{aligned}$$

In addition, from (3.16) and (3.10), together with (3.6), we obtain

$$\begin{aligned}
\alpha\,\|\boldsymbol{\delta}_h\|^2_{\mathbf{div};\Omega} \;\leq\; \alpha_1 \sum_{K\in\mathcal{T}_h}\Big\{&\|\Pi_k^h(\boldsymbol{\rho})-\boldsymbol{\mathcal{P}}_k^K(\boldsymbol{\rho})\|_{0,K}\|\boldsymbol{\delta}_h\|_{0,K}\\
&+\; \|\Pi_k^h(\boldsymbol{\rho})-\boldsymbol{\mathcal{P}}_k^K\big\{\Pi_k^h(\boldsymbol{\rho})\big\}\|_{0,K}\|\boldsymbol{\delta}_h-\boldsymbol{\mathcal{P}}_k^K(\boldsymbol{\delta}_h)\|_{0,K}\Big\}\\
&+\; \frac{2}{\mu}\sum_{K\in\mathcal{T}_h}\|\boldsymbol{\rho}-\boldsymbol{\mathcal{P}}_k^K(\boldsymbol{\rho})\|_{0,K}\|\boldsymbol{\delta}_h\|_{0,K}\,,
\end{aligned}$$

which yields

$$\|\boldsymbol{\delta}_h\|_{\mathbf{div};\Omega} \;\leq\; C\Big\{\|\boldsymbol{\rho}-\boldsymbol{\mathcal{P}}_k^h(\boldsymbol{\rho})\|_{0,\Omega} \;+\; \|\Pi_k^h(\boldsymbol{\rho})-\boldsymbol{\mathcal{P}}_k^h(\boldsymbol{\rho})\|_{0,\Omega} \;+\; \|\Pi_k^h(\boldsymbol{\rho})-\boldsymbol{\mathcal{P}}_k^h\big\{\Pi_k^h(\boldsymbol{\rho})\big\}\|_{0,\Omega}\Big\}\,. \tag{3.29}$$

with $C := \frac{2}{\alpha}\max\{\alpha_1,\frac{1}{\mu}\}$. Next, adding and subtracting $\boldsymbol{\rho}$, we deduce that

$$\|\Pi_k^h(\boldsymbol{\rho})-\boldsymbol{\mathcal{P}}_k^h(\boldsymbol{\rho})\|_{0,\Omega} \;\leq\; \|\boldsymbol{\rho}-\Pi_k^h(\boldsymbol{\rho})\|_{0,\Omega} \;+\; \|\boldsymbol{\rho}-\boldsymbol{\mathcal{P}}_k^h(\boldsymbol{\rho})\|_{0,\Omega}\,. \tag{3.30}$$

In turn, adding and subtracting $\boldsymbol{\rho}-\boldsymbol{\mathcal{P}}_k^h(\boldsymbol{\rho})$, and employing again the boundedness of $\boldsymbol{\mathcal{P}}_k^h$ (cf. (3.6)), we get

$$\begin{aligned}
\|\Pi_k^h(\boldsymbol{\rho})-\boldsymbol{\mathcal{P}}_k^h\big\{\Pi_k^h(\boldsymbol{\rho})\big\}\|_{0,\Omega} \;&\leq\; \|\boldsymbol{\rho}-\Pi_k^h(\boldsymbol{\rho})\|_{0,\Omega} \;+\; \|\boldsymbol{\rho}-\boldsymbol{\mathcal{P}}_k^h(\boldsymbol{\rho})\|_{0,\Omega} \;+\; \|\boldsymbol{\mathcal{P}}_k^h\big\{\boldsymbol{\rho}-\Pi_k^h(\boldsymbol{\rho})\big\}\|_{0,\Omega}\\
&\leq\; 2\,\|\boldsymbol{\rho}-\Pi_k^h(\boldsymbol{\rho})\|_{0,\Omega} \;+\; \|\boldsymbol{\rho}-\boldsymbol{\mathcal{P}}_k^h(\boldsymbol{\rho})\|_{0,\Omega}\,.
\end{aligned} \tag{3.31}$$

In this way, replacing (3.30) and (3.31) back into (3.29), and then the resulting estimate back into (3.28), we arrive at (3.25). On the other hand, concerning the error $\|\mathbf{u}-\mathbf{u}_h\|_{0,\Omega}$, we begin by using the triangle inequality,

$$\|\mathbf{u}-\mathbf{u}_h\|_{0,\Omega} \;\leq\; \|\mathbf{u}-\mathcal{P}_k^h(\mathbf{u})\|_{0,\Omega} \;+\; \|\mathcal{P}_k^h(\mathbf{u})-\mathbf{u}_h\|_{0,\Omega}\,. \tag{3.32}$$

Next, taking $\mathbf{v}_h := \mathcal{P}_k^h(\mathbf{u}) - \mathbf{u}_h \in \mathbf{Q}_h$ in the discrete inf-sup condition (3.20), we have

$$\|\mathcal{P}_k^h(\mathbf{u}) - \mathbf{u}_h\|_{0,\Omega} \;\leq\; \frac{1}{\beta} \sup_{\substack{\boldsymbol{\tau}_h \in \mathbb{H}_{0,h} \\ \boldsymbol{\tau}_h \neq \mathbf{0}}} \frac{b(\boldsymbol{\tau}_h, \mathcal{P}_k^h(\mathbf{u}) - \mathbf{u}_h)}{\|\boldsymbol{\tau}_h\|_{\mathbf{div};\Omega}} \,. \tag{3.33}$$

It follows, employing the definition of $\mathcal{P}_k^h : \mathbf{L}^2(\Omega) \to \mathbf{Q}_h$ ($\mathbf{L}^2(\Omega)$-orthogonal projector), the fact that $\boldsymbol{\tau}_h \in \mathbb{H}_{0,h}$ implies $\mathbf{div}(\boldsymbol{\tau}_h) \in \mathbf{Q}_h$, the first equations of (2.9) and (3.19), and (3.15), that

$$\begin{aligned} b(\boldsymbol{\tau}_h, \mathcal{P}_k^h(\mathbf{u}) - \mathbf{u}_h) \;&=\; \int_\Omega \mathcal{P}_k^h(\mathbf{u}) \cdot \mathbf{div}(\boldsymbol{\tau}_h) \;-\; b(\boldsymbol{\tau}_h, \mathbf{u}_h) \;=\; b(\boldsymbol{\tau}_h, \mathbf{u}) \;-\; b(\boldsymbol{\tau}_h, \mathbf{u}_h) \\ &=\; a_h(\boldsymbol{\rho}_h, \boldsymbol{\tau}_h) \;-\; a(\boldsymbol{\rho}, \boldsymbol{\tau}_h) \;=\; \sum_{K \in \mathcal{T}_h} \Big\{ a_h^K(\boldsymbol{\rho}_h - \boldsymbol{\mathcal{P}}_k^K(\boldsymbol{\rho}), \boldsymbol{\tau}_h) \,+\, a_h^K(\boldsymbol{\mathcal{P}}_k^K(\boldsymbol{\rho}), \boldsymbol{\tau}_h) \,-\, a^K(\boldsymbol{\rho}, \boldsymbol{\tau}_h) \Big\} \\ &=\; \sum_{K \in \mathcal{T}_h} \Big\{ a_h^K(\boldsymbol{\rho}_h - \boldsymbol{\mathcal{P}}_k^K(\boldsymbol{\rho}), \boldsymbol{\tau}_h) \;-\; a(\boldsymbol{\rho} - \boldsymbol{\mathcal{P}}_k^K(\boldsymbol{\rho}), \boldsymbol{\tau}_h) \Big\} \,, \end{aligned}$$

which, using that a_h^K (cf. (3.16)), a^K (cf. (3.10)) and $\boldsymbol{\mathcal{P}}_k^K$ (cf. (3.6)) are bounded, gives

$$b(\boldsymbol{\tau}_h, \mathcal{P}_k^h(\mathbf{u}) - \mathbf{u}_h) \;\leq\; C \Big\{ \|\boldsymbol{\rho} - \boldsymbol{\mathcal{P}}_k^h(\boldsymbol{\rho})\|_{0,\Omega} \,+\, \|\boldsymbol{\rho}_h - \boldsymbol{\mathcal{P}}_k^h(\boldsymbol{\rho})\|_{0,\Omega} \,+\, \|\boldsymbol{\rho}_h - \boldsymbol{\mathcal{P}}_k^h(\boldsymbol{\rho}_h)\|_{0,\Omega} \Big\} \|\boldsymbol{\tau}_h\|_{0,\Omega} \,.$$

Therefore, replacing the above identity in (3.33) yields

$$\|\mathcal{P}_k^h(\mathbf{u}) - \mathbf{u}_h\|_{0,\Omega} \;\leq\; C \Big\{ \|\boldsymbol{\rho} - \boldsymbol{\mathcal{P}}_k^h(\boldsymbol{\rho})\|_{0,\Omega} \,+\, \|\boldsymbol{\rho}_h - \boldsymbol{\mathcal{P}}_k^h(\boldsymbol{\rho})\|_{0,\Omega} \,+\, \|\boldsymbol{\rho}_h - \boldsymbol{\mathcal{P}}_k^h(\boldsymbol{\rho}_h)\|_{0,\Omega} \Big\} \,. \tag{3.34}$$

Thus, adding and subtracting $\boldsymbol{\rho}$, we readily get

$$\|\boldsymbol{\rho}_h - \boldsymbol{\mathcal{P}}_k^h(\boldsymbol{\rho})\|_{0,\Omega} \;\leq\; \|\boldsymbol{\rho} - \boldsymbol{\rho}_h\|_{0,\Omega} \,+\, \|\boldsymbol{\rho} - \boldsymbol{\mathcal{P}}_k^h(\boldsymbol{\rho})\|_{0,\Omega} \,. \tag{3.35}$$

Similarly, adding and subtracting $\boldsymbol{\rho} - \boldsymbol{\mathcal{P}}_k^h(\boldsymbol{\rho})$, and utilizing once again the boundedness of $\boldsymbol{\mathcal{P}}_k^K$ (cf. (3.6)), we obtain

$$\begin{aligned} \|\boldsymbol{\rho}_h - \boldsymbol{\mathcal{P}}_k^h(\boldsymbol{\rho}_h)\|_{0,\Omega} \;&\leq\; \|\boldsymbol{\rho} - \boldsymbol{\rho}_h\|_{0,\Omega} \,+\, \|\boldsymbol{\rho} - \boldsymbol{\mathcal{P}}_k^h(\boldsymbol{\rho})\|_{0,\Omega} \,+\, \|\boldsymbol{\mathcal{P}}_k^h(\boldsymbol{\rho} - \boldsymbol{\rho}_h)\|_{0,\Omega} \\ &\leq\; 2\,\|\boldsymbol{\rho} - \boldsymbol{\rho}_h\|_{0,\Omega} \,+\, \|\boldsymbol{\rho} - \boldsymbol{\mathcal{P}}_k^h(\boldsymbol{\rho})\|_{0,\Omega} \,. \end{aligned} \tag{3.36}$$

Finally, the estimate (3.27) follows after putting (3.32), (3.34), (3.35), (3.36), and (3.25) together. □

Having established the *a priori* error estimates for our unknowns, we now provide the corresponding rates of convergence.

Theorem 3.3. *Let $(\boldsymbol{\rho}, \mathbf{u}) \in \mathbb{H}_0 \times \mathbf{Q}$ and $(\boldsymbol{\rho}_h, \mathbf{u}_h) \in \mathbb{H}_{0,h} \times \mathbf{Q}_h$ be the unique solutions of the continuous and discrete schemes* (2.9) *and* (3.19)*, respectively. Assume that for some $r \in [1, k+1]$ there hold $\boldsymbol{\rho}|_K \in \mathbb{H}^r(K)$, $\mathbf{div}(\boldsymbol{\rho})|_K \in \mathbf{H}^r(K)$, and $\mathbf{u}|_K \in \mathbf{H}^r(K)$ for each $K \in \mathcal{T}_h$. Then, there exist positive constants C_1, C_2, independent of h and λ, such that*

$$\|\boldsymbol{\rho} - \boldsymbol{\rho}_h\|_{\mathbf{div};\Omega} \,\leq\, C_1\, h^r \sum_{K \in \mathcal{T}_h} \Big\{ |\boldsymbol{\rho}|_{r,K} \,+\, |\mathbf{div}(\boldsymbol{\rho})|_{r,K} \Big\} \,,$$

and

$$\|\mathbf{u} - \mathbf{u}_h\|_{0,\Omega} \,\leq\, C_2\, h^r \sum_{K \in \mathcal{T}_h} \Big\{ |\boldsymbol{\rho}|_{r,K} \,+\, |\mathbf{u}|_{r,K} \Big\} \,.$$

Proof. It follows from a straightforward application of the approximation properties provided by (3.7), (3.22), (3.23) and (3.24), to the terms on the right-hand sides of (3.25), (3.26) and (3.27). □

4 Computable approximations of $\boldsymbol{\rho}$ and $\boldsymbol{\sigma}$

In this section we introduce fully computable approximations of $\boldsymbol{\rho}$ and $\boldsymbol{\sigma}$, and establish the corresponding a priori error estimates and consequent rates of convergence.

4.1 Convergent approximations of $\boldsymbol{\rho}$ and $\boldsymbol{\sigma}$ in the $\mathbb{L}^2$-norm

We follow [13, 14] and set the approximation of $\boldsymbol{\rho}$ given by

$$\widehat{\boldsymbol{\rho}}_h \;:=\; \boldsymbol{\mathcal{P}}_k^h(\boldsymbol{\rho}_h)\,. \tag{4.1}$$

Then, in what follows we show that $\boldsymbol{\rho}_h$ and $\widehat{\boldsymbol{\rho}}_h$ share the same rates of convergence given by Theorem 3.3 with respect to the norm $\|\cdot\|_{0,\Omega}$.

Lemma 4.1. *There exists a positive constant C, independent of h and λ, such that*

$$\|\boldsymbol{\rho}-\widehat{\boldsymbol{\rho}}_h\|_{0,\Omega} \;\leq\; C\Big\{\|\boldsymbol{\rho}-\Pi_k^h(\boldsymbol{\rho})\|_{0,\Omega} \;+\; \|\boldsymbol{\rho}-\boldsymbol{\mathcal{P}}_k^h(\boldsymbol{\rho})\|_{0,\Omega}\Big\}\,. \tag{4.2}$$

Proof. Similarly as in [13, Theorem 5.4], we add and subtract $\boldsymbol{\rho}_h$ to obtain

$$\|\boldsymbol{\rho}-\widehat{\boldsymbol{\rho}}_h\|_{0,\Omega} \;\leq\; \|\boldsymbol{\rho}-\boldsymbol{\rho}_h\|_{0,\Omega} \;+\; \|\boldsymbol{\rho}_h-\boldsymbol{\mathcal{P}}_k^h(\boldsymbol{\rho}_h)\|_{0,\Omega}\,.$$

Then, using (3.36) and (3.25), we arrive at (4.2) and complete the proof. □

Next, as suggested by the identity (2.10), we approximate the symmetric tensor field $\boldsymbol{\sigma}$ by the postprocessing formula

$$\widehat{\boldsymbol{\sigma}}_h \;:=\; \widehat{\boldsymbol{\rho}}_h \;+\; (\widehat{\boldsymbol{\rho}}_h)^{\mathtt{t}} \;-\; \left\{\frac{\lambda+2\mu}{2\lambda+3\mu}\,\mathrm{tr}(\widehat{\boldsymbol{\rho}}_h) - \frac{\lambda+\mu}{|\Omega|}\int_\Gamma \mathbf{g}\cdot\boldsymbol{n}\right\}\mathbb{I}\,. \tag{4.3}$$

Hence, using (2.10) and the fact that $\frac{\lambda+2\mu}{2\lambda+3\mu}<1$, we readily find that

$$\|\boldsymbol{\sigma}-\widehat{\boldsymbol{\sigma}}_h\|_{0,\Omega} \;\leq\; 4\,\|\boldsymbol{\rho}-\widehat{\boldsymbol{\rho}}_h\|_{0,\Omega}\,, \tag{4.4}$$

which shows that the a priori error estimate for $\|\boldsymbol{\sigma}-\widehat{\boldsymbol{\sigma}}_h\|_{0,\Omega}$ follows from that of $\|\boldsymbol{\rho}-\widehat{\boldsymbol{\rho}}_h\|_{0,\Omega}$ (cf. Lemma 4.1). Moreover, the following theorem provides the corresponding rates of convergence.

Theorem 4.1. *Let $(\boldsymbol{\rho},\mathbf{u})\in\mathbb{H}_0\times\mathbf{Q}$ and $(\boldsymbol{\rho}_h,\mathbf{u}_h)\in\mathbb{H}_{0,h}\times\mathbf{Q}_h$ be the unique solutions of the continuous and discrete schemes* (2.9) *and* (3.19)*, respectively. In addition, let $\boldsymbol{\sigma}$ be the stress tensor given by* (2.10) *and let $\widehat{\boldsymbol{\rho}}_h$ and $\widehat{\boldsymbol{\sigma}}_h$ be the discrete approximations introduced in* (4.1) *and* (4.3)*, respectively. Assume that for some $r\in[1,k+1]$ there holds $\boldsymbol{\rho}|_K\in\mathbb{H}^r(K)$ for each $K\in\mathcal{T}_h$. Then, there exists a positive constant C, independent of h and λ, such that*

$$\|\boldsymbol{\rho}-\widehat{\boldsymbol{\rho}}_h\|_{0,\Omega} \;+\; \|\boldsymbol{\sigma}-\widehat{\boldsymbol{\sigma}}_h\|_{0,\Omega} \;\leq\; C\,h^r\sum_{K\in\mathcal{T}_h}|\boldsymbol{\rho}|_{r,K}\,.$$

Proof. It is clear from (4.4) and Lemma 4.1 that

$$\|\boldsymbol{\rho}-\widehat{\boldsymbol{\rho}}_h\|_{0,\Omega} \;+\; \|\boldsymbol{\sigma}-\widehat{\boldsymbol{\sigma}}_h\|_{0,\Omega} \;\leq\; C\Big\{\|\boldsymbol{\rho}-\Pi_k^h(\boldsymbol{\rho})\|_{0,\Omega} \;+\; \|\boldsymbol{\rho}-\boldsymbol{\mathcal{P}}_k^h(\boldsymbol{\rho})\|_{0,\Omega}\Big\}\,,$$

which, together with the approximation properties (3.7) and (3.23), complete the proof. □

4.2 Convergent approximations of $\boldsymbol{\rho}$ and $\boldsymbol{\sigma}$ in the broken $\mathbb{H}(\mathbf{div})$-norm

Some preliminary numerical experiments confirm that the rates of convergence of the errors

$$\left\{ \sum_{K\in\mathcal{T}_h} \|\boldsymbol{\rho}-\widehat{\boldsymbol{\rho}}_h\|^2_{\mathbf{div};K} \right\}^{1/2}, \quad \text{and} \quad \left\{ \sum_{K\in\mathcal{T}_h} \|\boldsymbol{\sigma}-\widehat{\boldsymbol{\sigma}}_h\|^2_{\mathbf{div};K} \right\}^{1/2}$$

are smaller, by a power of h, than the ones associated to $\|\boldsymbol{\sigma}-\widehat{\boldsymbol{\sigma}}_h\|_{0,\Omega}$ and $\|\boldsymbol{\rho}-\widehat{\boldsymbol{\rho}}_h\|_{0,\Omega}$. This fact has motivated the construction of new, improved, approximations to the tensors $\boldsymbol{\rho}$ and $\boldsymbol{\sigma}$, having better rates of convergence with respect to the broken $\mathbb{H}(\mathbf{div})$-norm. In order to do this, we follow the postprocessing techniques presented in [14, 15, 20, 21]. Indeed, given $K\in\mathcal{T}_h$, and denoting the usual $\mathbb{H}(\mathbf{div};K)$-inner product by $(\cdot,\cdot)_{\mathbf{div};K}$, we define $\widehat{\boldsymbol{\rho}}^\star_h|_K := \widehat{\boldsymbol{\rho}}^\star_{h,K}\in\mathbb{P}_{k+1}(K)$ and $\widehat{\boldsymbol{\sigma}}^\star_h|_K := \widehat{\boldsymbol{\sigma}}^\star_{h,K}\in\mathbb{P}_{k+1}(K)$, as the solutions of the local problems

$$(\widehat{\boldsymbol{\rho}}^\star_{h,K},\boldsymbol{\tau}_h)_{\mathbf{div};K} = \int_K \widehat{\boldsymbol{\rho}}_h:\boldsymbol{\tau}_h - \int_K \mathbf{f}\cdot\mathbf{div}(\boldsymbol{\tau}_h) \qquad \forall\,\boldsymbol{\tau}_h\in\mathbb{P}_{k+1}(K), \tag{4.5}$$

and

$$(\widehat{\boldsymbol{\sigma}}^\star_{h,K},\boldsymbol{\tau}_h)_{\mathbf{div};K} = \int_K \widehat{\boldsymbol{\sigma}}_h:\boldsymbol{\tau}_h - \int_K \mathbf{f}\cdot\mathbf{div}(\boldsymbol{\tau}_h) \qquad \forall\,\boldsymbol{\tau}_h\in\mathbb{P}_{k+1}(K), \tag{4.6}$$

where both identities above have taken advantage of the fact that $\mathbf{div}(\boldsymbol{\rho})=\mathbf{div}(\boldsymbol{\sigma})=-\mathbf{f}$. In turn, we could have replaced in both right-hand sides the term $-\int_K \mathbf{f}\cdot\mathbf{div}(\boldsymbol{\tau}_h)$ by $\int_K \mathbf{div}(\boldsymbol{\rho}_h)\cdot\mathbf{div}(\boldsymbol{\tau}_h)$, with $\boldsymbol{\rho}_h\in\mathbb{H}_{0,h}$ given by the discrete scheme (3.19). These alternative choices yield the same rate of convergence, but we prefer to use $-\mathbf{f}$ instead of $\mathbf{div}(\boldsymbol{\rho}_h)$, as this gives precisely the exact value of the divergence of $\boldsymbol{\rho}$ and $\boldsymbol{\sigma}$.

The following result provides the global rates of convergence for $\widehat{\boldsymbol{\rho}}^\star_h$ and $\widehat{\boldsymbol{\sigma}}^\star_h$.

Theorem 4.2. *Let $(\boldsymbol{\rho},\mathbf{u})\in\mathbb{H}_0\times\mathbf{Q}$ and $(\boldsymbol{\rho}_h,\mathbf{u}_h)\in\mathbb{H}_{0,h}\times\mathbf{Q}_h$ be the unique solutions of the continuous and discrete schemes* (2.9) *and* (3.19)*, respectively. In addition, let $\boldsymbol{\sigma}$ be the stress tensor given by* (2.10) *and let $\widehat{\boldsymbol{\rho}}_h$, $\widehat{\boldsymbol{\sigma}}_h$, $\widehat{\boldsymbol{\rho}}^\star_h$, and $\widehat{\boldsymbol{\sigma}}^\star_h$ be the discrete approximations introduced in* (4.1), (4.3), (4.5) *and* (4.6)*, respectively. Assume that for some $r\in[1,k+1]$ there hold $\boldsymbol{\rho}|_K\in\mathbb{H}^r(K)$ and $\mathbf{div}(\boldsymbol{\rho})|_K\in\mathbf{H}^r(K)$ for each $K\in\mathcal{T}_h$. Then, there exists a positive constant C, independent of h and λ, such that*

$$\left\{ \sum_{K\in\mathcal{T}_h} \|\boldsymbol{\rho}-\widehat{\boldsymbol{\rho}}^\star_h\|^2_{\mathbf{div};K} \right\}^{1/2} + \left\{ \sum_{K\in\mathcal{T}_h} \|\boldsymbol{\sigma}-\widehat{\boldsymbol{\sigma}}^\star_h\|^2_{\mathbf{div};K} \right\}^{1/2} \leq C\,h^r \sum_{K\in\mathcal{T}_h} \Big\{ |\boldsymbol{\rho}|_{r,K} + |\mathbf{div}(\boldsymbol{\rho})|_{r,K} \Big\}.$$

Proof. It follows similarly as in [14, Theorem 4.4] and [21, Theorem 3.3]. □

5 Numerical results

In this section we present some numerical results illustrating the performance of the mixed virtual element scheme (3.19), introduced and analyzed in Section 3. For all the computations we consider the specific virtual element subspaces $\mathbb{H}_{0,h}$ and $\mathbf{Q}_h$ given by (3.2) and (3.3) with $k\in\{0,1,2\}$. In addition, and similarly as in [14] and [17], the zero integral mean condition for tensors in the space $\mathbb{H}_{0,h}$ is imposed via a real Lagrange multiplier. Concerning the decompositions of Ω employed in our computations, we follow [14] and consider uniform triangles, distorted squares and quasi-uniform hexagons as decompositions of the domain.

We begin by introducing some notations. In what follows, N stands for the total number of degrees of freedom (unknowns) of (3.19). In this case, we have that

$$N \ := \ 2(k+1) \times \{\# \text{ of edges in } \mathcal{T}_h\} \ + \ (3k+1)(k+2) \times \{\# \text{ of elements in } \mathcal{T}_h\} \ + \ 1 \, .$$

In turn, the individual errors for all the unknowns are given by

$$\mathtt{e}(\boldsymbol{\rho}) \ := \ \|\boldsymbol{\rho} - \widehat{\boldsymbol{\rho}}_h\|_{0,\Omega} \, , \qquad \mathtt{e}(\mathbf{u}) \ := \ \|\mathbf{u} - \mathbf{u}_h\|_{0,\Omega} \, , \qquad \mathtt{e}(\boldsymbol{\sigma}) \ := \ \|\boldsymbol{\sigma} - \widehat{\boldsymbol{\sigma}}_h\|_{0,\Omega} \, ,$$

$$\mathtt{e}(\boldsymbol{\rho}^\star) \ := \ \left\{ \sum_{K \in \mathcal{T}_h} \|\boldsymbol{\rho} - \widehat{\boldsymbol{\rho}}_h^\star\|^2_{\mathbf{div};K} \right\}^{1/2} \quad \text{and} \quad \mathtt{e}(\boldsymbol{\sigma}^\star) \ := \ \left\{ \sum_{K \in \mathcal{T}_h} \|\boldsymbol{\sigma} - \widehat{\boldsymbol{\sigma}}_h^\star\|^2_{\mathbf{div};K} \right\}^{1/2} ,$$

where $\widehat{\boldsymbol{\rho}}_h$, $\widehat{\boldsymbol{\sigma}}_h$, $\widehat{\boldsymbol{\rho}}_h^\star$, and $\widehat{\boldsymbol{\sigma}}_h^\star$ are computed according to (4.1), (4.3), (4.5), and (4.6), respectively. Then, we define the experimental rates of convergence

$$\mathtt{r}(\cdot) \ := \ \frac{\log\big(\mathtt{e}(\cdot) \, / \, \mathtt{e}'(\cdot)\big)}{\log(h \, / \, h')} \, ,$$

where $\mathtt{e}$ and $\mathtt{e}'$ denote the corresponding errors for two consecutive meshes with sizes h and h', respectively. The numerical results presented below were obtained using a MATLAB code, where the corresponding linear systems were solved using its instruction "\" as main solver.

Next, we recall that given the Young modulus E and the Poisson ratio ν of an isotropic linear elastic solid, the corresponding Lamé parameters are defined as

$$\mu \ := \ \frac{E}{2(1+\nu)} \quad \text{and} \quad \lambda \ := \ \frac{E\nu}{(1+\nu)(1-2\nu)} \, .$$

In the examples below, we follow [17, 21, 22] by fixing $E = 1$ and taking $\nu \in \{0.3000, 0.4900, 0.4999\}$, and summarize the values of μ and λ in the following table:

ν	μ	λ
0.3000	0.3846	0.5769
0.4900	0.3356	16.4430
0.4999	0.3333	1666.4444

It is important to remark here that the cases $\nu = 0.4900$ and $\nu = 0.4999$ correspond to materials showing nearly incompressible behaviour.

In what follows, we take the domain Ω to be either the unit square $(0,1)^2$ or the L-shaped domain $(-1,1)^2 \setminus [0,1]^2$, and choose $\mathbf{f}$ and $\mathbf{g}$ so that the Poisson ratio ν and the exact solution $\mathbf{u}$ are given as follows:

Example	Ω	ν	$\mathbf{u}(x_1, x_2)$
1	Unit square	0.4900	$\begin{pmatrix} \sin(2\pi x_1)\cos(2\pi x_2) \\ \cos(2\pi x_1)\sin(2\pi x_2) \end{pmatrix}$
2	L-shaped	0.3000	$\begin{pmatrix} r^{2/3}\sin(\theta) \\ -r^{2/3}\cos(\theta) \end{pmatrix}$
3	Unit square	0.4999	$x_1 x_2 (1-x_1)(1-x_2) e^{x_1+x_2} \begin{pmatrix} 1 \\ 1 \end{pmatrix}$

where $r := \sqrt{x_1^2 + x_2^2}$ and $\theta := \arctan\left(\frac{x_2}{x_1}\right)$ in Example 2. Note that the solution of Example 2 is singular at the origin, so that we should expect high gradients around the origin.

In Tables 5.1 up to 5.3, we summarize the convergence history of the mixed virtual element scheme (3.19) applied to Example 1. We notice there that the rate of convergence $O(h^{k+1})$ predicted by Theorems 3.3, 4.1 and 4.2 (when $r = k+1$) is attained for all the unknowns for this smooth example, for triangular as well as for quadrilateral and hexagonal meshes. In particular, these results confirm that our postprocessed stress $\boldsymbol{\sigma}_h^\star$ improves in one power the non-satisfactory order provided by the first approximation $\boldsymbol{\sigma}_h$ with respect to the broken $\mathbb{H}(\mathbf{div})$-norm. In addition, as observed in the seventh column of Tables 5.1−5.3, the convergence of $\mathtt{e}(\mathbf{u})$ is a bit faster than expected, which seems a special behaviour of this particular solution $\mathbf{u}$. Next, in Tables 5.4 up to 5.6, we provide the convergence history of Example 2. In this case, and because of the singularity at the origin of the exact solution, the theoretical orders of convergence are not attained. In fact, it is easy to show that $\mathbf{u}$ belong to $\mathbf{H}^{5/3}(\Omega)$, whence $\boldsymbol{\rho}, \boldsymbol{\sigma} \in \mathbb{H}^{2/3}(\Omega)$ and $\mathbf{div}(\boldsymbol{\rho}) = \mathbf{div}(\boldsymbol{\sigma}) \in \mathbf{H}^{-1/3}(\Omega)$. Thus, thanks to Theorems 3.3, 4.1 and 4.2, we can explain the *a priori* estimates in Tables 5.4−5.6 for $\boldsymbol{\rho}$, $\mathbf{u}$, $\boldsymbol{\sigma}$ and also for $\mathtt{e}(\boldsymbol{\rho}^\star)$ and $\mathtt{e}(\boldsymbol{\sigma}^\star)$. Finally, the convergence history for Example 3 is presented in Tables 5.7 up to 5.9, where we obtained the same results as in Example 1. Furthermore, we remark here that Example 3 used $\nu = 0.4999$, which as mentioned in advance, corresponds to materials showing nearly incompressible behaviour. Nonetheless, our mixed-VEM scheme (3.19) seems to be able to solve this problem without difficulties.

We end this paper by displaying some components of the approximate solutions for the three examples, in Figures 5.1 to 5.6. They all correspond to those obtained with the first mesh of each kind (triangles, quadrilaterals and hexagons, respectively) and for the polynomial degree $k = 2$. Here we use the notations $\boldsymbol{\rho}_h = (\rho_{h,ij})_{i,j=1,2}$, $\boldsymbol{\sigma}_h = (\sigma_{h,ij})_{i,j=1,2}$, and $\mathbf{u}_h = (u_{h,i})_{i=1,2}$.

k	h	N	$\mathtt{e}(\boldsymbol{\rho})$	$\mathtt{r}(\boldsymbol{\rho})$	$\mathtt{e}(\mathbf{u})$	$\mathtt{r}(\mathbf{u})$	$\mathtt{e}(\boldsymbol{\sigma})$	$\mathtt{r}(\boldsymbol{\sigma})$	$\mathtt{e}(\boldsymbol{\rho}^\star)$	$\mathtt{r}(\boldsymbol{\rho}^\star)$	$\mathtt{e}(\boldsymbol{\sigma}^\star)$	$\mathtt{r}(\boldsymbol{\sigma}^\star)$
	0.0643	4929	1.98e+1	−−	8.61e-1	−−	2.68e+1	−−	9.27e+1	−−	9.44e+1	−−
	0.0488	8527	1.48e+1	1.06	5.10e-1	1.90	2.03e+1	1.00	7.03e+1	1.00	7.17e+1	1.00
0	0.0248	32719	7.36e-0	1.03	1.37e-1	1.94	1.03e+1	1.00	3.58e+1	1.00	3.65e+1	1.00
	0.0166	72591	4.92e-0	1.01	6.35e-2	1.93	6.91e-0	1.00	2.40e+1	1.00	2.45e+1	1.00
	0.0129	121441	3.79e-0	1.01	3.89e-2	1.90	5.34e-0	1.00	1.85e+1	1.00	1.89e+1	1.00
	0.0643	17601	9.58e-1	−−	1.68e-2	−−	1.15e-0	−−	5.09e-0	−−	5.13e-0	−−
	0.0488	30509	5.62e-1	1.93	7.73e-3	2.81	6.86e-1	1.88	2.94e-0	1.99	2.96e-0	1.99
1	0.0248	117421	1.49e-1	1.96	1.17e-3	2.80	1.86e-1	1.93	7.62e-1	2.00	7.70e-1	1.99
	0.0166	260781	6.76e-2	1.98	4.01e-4	2.67	8.49e-2	1.97	3.43e-1	2.00	3.47e-1	2.00
	0.0129	436481	4.05e-2	1.99	2.09e-4	2.54	5.09e-2	1.98	2.05e-1	2.00	2.07e-1	2.00
	0.0643	36081	3.79e-2	−−	4.68e-4	−−	4.08e-2	−−	2.05e-1	−−	2.06e-1	−−
	0.0488	62583	1.66e-2	3.00	1.60e-4	3.88	1.78e-2	3.00	8.97e-2	3.00	8.99e-2	3.00
2	0.0248	241111	2.18e-3	3.00	1.30e-5	3.71	2.34e-3	3.00	1.18e-2	3.00	1.19e-2	3.00
	0.0166	535671	6.58e-4	3.00	3.26e-6	3.46	7.07e-4	3.00	3.57e-3	3.00	3.58e-3	3.00
	0.0129	896721	3.04e-4	3.00	1.39e-6	3.31	3.26e-4	3.00	1.65e-3	3.00	1.65e-3	3.00

Table 5.1: Example 1, history of convergence using triangles.

k	h	N	$\mathtt{e}(\boldsymbol{\rho})$	$\mathtt{r}(\boldsymbol{\rho})$	$\mathtt{e}(\mathbf{u})$	$\mathtt{r}(\mathbf{u})$	$\mathtt{e}(\boldsymbol{\sigma})$	$\mathtt{r}(\boldsymbol{\sigma})$	$\mathtt{e}(\boldsymbol{\rho}^\star)$	$\mathtt{r}(\boldsymbol{\rho}^\star)$	$\mathtt{e}(\boldsymbol{\sigma}^\star)$	$\mathtt{r}(\boldsymbol{\sigma}^\star)$
	0.0716	5521	1.56e+1	−−	7.16e-1	−−	1.61e+1	−−	9.24e+1	−−	9.25e+1	−−
	0.0537	9761	1.08e+1	1.28	3.73e-1	2.27	1.09e+1	1.35	6.67e+1	1.13	6.68e+1	1.13
0	0.0286	34051	5.31e-0	1.13	9.70e-2	2.14	5.29e-0	1.16	3.40e+1	1.07	3.40e+1	1.07
	0.0195	73041	3.56e-0	1.04	4.54e-2	1.99	3.53e-0	1.05	2.29e+1	1.03	2.29e+1	1.03
	0.0148	126731	2.69e-0	1.02	2.70e-2	1.87	2.66e-0	1.03	1.73e+1	1.02	1.73e+1	1.02
	0.0716	18241	8.87e-1	−−	1.60e-2	−−	8.84e-1	−−	5.64e-0	−−	5.63e-0	−−
	0.0537	32321	4.53e-1	2.34	6.36e-3	3.21	4.50e-1	2.35	2.89e-0	2.32	2.89e-0	2.32
1	0.0286	113101	1.14e-1	2.20	9.55e-4	3.02	1.13e-1	2.20	7.29e-1	2.19	7.29e-1	2.19
	0.0195	242881	5.10e-2	2.10	3.37e-4	2.72	5.05e-2	2.10	3.27e-1	2.09	3.27e-1	2.09
	0.0148	421661	2.89e-2	2.06	1.69e-4	2.50	2.86e-2	2.06	1.85e-1	2.06	1.85e-1	2.06
	0.0716	36361	4.08e-2	−−	3.55e-4	−−	4.04e-2	−−	2.43e-1	−−	2.43e-1	−−
	0.0537	64481	1.45e-2	3.60	1.04e-4	4.27	1.44e-2	3.60	8.77e-2	3.54	8.77e-2	3.54
2	0.0286	225901	1.73e-3	3.38	9.41e-6	3.82	1.72e-3	3.38	1.07e-2	3.34	1.07e-2	3.34
	0.0195	485321	5.08e-4	3.20	2.55e-6	3.41	5.03e-4	3.20	3.17e-3	3.18	3.17e-3	3.18
	0.0148	842741	2.14e-4	3.14	1.04e-6	3.25	2.12e-4	3.14	1.34e-3	3.12	1.34e-3	3.12

Table 5.2: Example 1, history of convergence using quadrilaterals.

k	h	N	$\mathtt{e}(\boldsymbol{\rho})$	$\mathtt{r}(\boldsymbol{\rho})$	$\mathtt{e}(\mathbf{u})$	$\mathtt{r}(\mathbf{u})$	$\mathtt{e}(\boldsymbol{\sigma})$	$\mathtt{r}(\boldsymbol{\sigma})$	$\mathtt{e}(\boldsymbol{\rho}^\star)$	$\mathtt{r}(\boldsymbol{\rho}^\star)$	$\mathtt{e}(\boldsymbol{\sigma}^\star)$	$\mathtt{r}(\boldsymbol{\sigma}^\star)$
	0.0414	8147	1.25e+1	−−	3.29e-1	−−	1.24e+1	−−	7.76e+1	−−	7.75e+1	−−
	0.0319	13563	9.56e-0	1.03	2.01e-1	1.91	9.51e-0	1.03	6.00e+1	0.99	6.00e+1	0.99
0	0.0235	24579	7.01e-0	1.02	1.11e-1	1.93	6.95e-0	1.03	4.43e+1	0.99	4.43e+1	0.99
	0.0167	48603	4.95e-0	1.01	5.83e-2	1.88	4.91e-0	1.01	3.14e+1	1.00	3.14e+1	1.00
	0.0124	88637	3.65e-0	1.01	3.40e-2	1.79	3.63e-0	1.01	2.33e+1	1.00	2.33e+1	1.00
	0.0414	24437	4.97e-1	−−	6.80e-3	−−	4.93e-1	−−	3.15e-0	−−	3.15e-0	−−
	0.0319	40757	2.96e-1	1.99	3.27e-3	2.82	2.94e-1	2.00	1.88e-0	1.98	1.88e-0	1.98
1	0.0235	73733	1.61e-1	2.00	1.41e-3	2.75	1.60e-1	2.00	1.03e-0	1.99	1.03e-0	1.99
	0.0167	145805	8.10e-2	2.00	5.72e-4	2.63	8.02e-2	2.00	5.17e-1	1.99	5.17e-1	1.99
	0.0124	266089	4.44e-2	2.00	2.71e-4	2.48	4.40e-2	2.00	2.83e-1	2.00	2.83e-1	2.00
	0.0414	46835	1.55e-2	−−	1.48e-4	−−	1.61e-2	−−	8.90e-2	−−	8.91e-2	−−
	0.0319	78175	7.16e-3	2.98	5.63e-5	3.72	7.43e-3	2.97	4.11e-2	2.98	4.11e-2	2.98
2	0.0235	141319	2.87e-3	2.99	1.86e-5	3.63	2.98e-3	2.99	1.65e-2	2.99	1.65e-2	2.99
	0.0167	279457	1.02e-3	2.99	5.62e-6	3.48	1.06e-3	2.99	5.89e-3	2.99	5.90e-3	2.99
	0.0124	510153	4.16e-4	2.99	2.06e-6	3.33	4.33e-4	2.99	2.39e-3	3.00	2.40e-3	3.00

Table 5.3: Example 1, history of convergence using hexagons.

k	h	N	$\mathtt{e}(\boldsymbol{\rho})$	$\mathtt{r}(\boldsymbol{\rho})$	$\mathtt{e}(\mathbf{u})$	$\mathtt{r}(\mathbf{u})$	$\mathtt{e}(\boldsymbol{\sigma})$	$\mathtt{r}(\boldsymbol{\sigma})$	$\mathtt{e}(\boldsymbol{\rho}^\star)$	$\mathtt{r}(\boldsymbol{\rho}^\star)$	$\mathtt{e}(\boldsymbol{\sigma}^\star)$	$\mathtt{r}(\boldsymbol{\sigma}^\star)$
	0.1179	4417	5.05e-2	−−	4.70e-2	−−	6.39e-2	−−	2.03e-0	−−	2.03e-0	−−
	0.0786	9865	3.89e-2	0.64	3.14e-2	1.00	4.95e-2	0.63	2.32e-0	-0.33	2.32e-0	-0.33
0	0.0429	32935	2.62e-2	0.65	1.71e-2	1.00	3.35e-2	0.64	2.84e-0	-0.33	2.84e-0	-0.33
	0.0289	72423	2.03e-2	0.65	1.15e-2	1.00	2.59e-2	0.65	3.24e-0	-0.33	3.24e-0	-0.33
	0.0218	127271	1.68e-2	0.66	8.68e-3	1.00	2.16e-2	0.65	3.56e-0	-0.33	3.56e-0	-0.33
	0.1179	15745	2.13e-2	−−	1.16e-3	−−	2.92e-2	−−	1.89e-0	−−	1.89e-0	−−
	0.0786	35281	1.63e-2	0.67	5.96e-4	1.64	2.23e-2	0.67	2.16e-0	-0.33	2.16e-0	-0.33
1	0.0429	118141	1.09e-2	0.67	2.21e-4	1.64	1.49e-2	0.67	2.64e-0	-0.33	2.64e-0	-0.33
	0.0289	260093	8.34e-3	0.67	1.15e-4	1.64	1.14e-2	0.67	3.02e-0	-0.33	3.02e-0	-0.33
	0.0218	457341	6.91e-3	0.67	7.27e-5	1.64	9.48e-3	0.67	3.32e-0	-0.33	3.32e-0	-0.33
	0.1179	32257	1.57e-2	−−	4.07e-4	−−	2.12e-2	−−	1.79e-0	−−	1.79e-0	−−
	0.0786	72361	1.20e-2	0.67	2.08e-4	1.65	1.62e-2	0.67	2.05e-0	-0.33	2.05e-0	-0.33
2	0.0429	242551	7.99e-3	0.67	7.67e-5	1.65	1.08e-2	0.67	2.51e-0	-0.33	2.51e-0	-0.33
	0.0289	534199	6.14e-3	0.67	4.01e-5	1.64	8.30e-3	0.67	2.86e-0	-0.33	2.86e-0	-0.33
	0.0218	939511	5.09e-3	0.67	2.53e-5	1.63	6.87e-3	0.67	3.14e-0	-0.33	3.14e-0	-0.33

Table 5.4: Example 2, history of convergence using triangles.

k	h	N	$\mathtt{e}(\boldsymbol{\rho})$	$\mathtt{r}(\boldsymbol{\rho})$	$\mathtt{e}(\mathbf{u})$	$\mathtt{r}(\mathbf{u})$	$\mathtt{e}(\boldsymbol{\sigma})$	$\mathtt{r}(\boldsymbol{\sigma})$	$\mathtt{e}(\boldsymbol{\rho}^\star)$	$\mathtt{r}(\boldsymbol{\rho}^\star)$	$\mathtt{e}(\boldsymbol{\sigma}^\star)$	$\mathtt{r}(\boldsymbol{\sigma}^\star)$
	0.1667	2689	5.14e-2	−−	6.64e-2	−−	7.58e-2	−−	2.16e-0	−−	2.16e-0	−−
	0.0927	8889	3.37e-2	0.72	3.38e-2	1.15	4.88e-2	0.75	2.56e-0	-0.29	2.56e-0	-0.29
0	0.0478	33627	2.16e-2	0.67	1.67e-2	1.06	3.10e-2	0.69	3.20e-0	-0.34	3.20e-0	-0.34
	0.0321	74241	1.67e-2	0.66	1.12e-2	1.02	2.38e-2	0.67	3.68e-0	-0.35	3.68e-0	-0.35
	0.0239	133817	1.37e-2	0.66	8.27e-3	1.02	1.96e-2	0.66	4.08e-0	-0.35	4.08e-0	-0.35
	0.1667	8833	2.93e-2	−−	2.21e-3	−−	4.31e-2	−−	2.24e-0	−−	2.24e-0	−−
	0.0927	29393	1.88e-2	0.76	7.43e-4	1.86	2.75e-2	0.76	2.65e-0	-0.29	2.65e-0	-0.29
1	0.0478	111629	1.19e-2	0.69	2.41e-4	1.70	1.74e-2	0.69	3.33e-0	-0.34	3.33e-0	-0.34
	0.0321	246785	9.15e-3	0.67	1.27e-4	1.63	1.33e-2	0.67	3.82e-0	-0.35	3.83e-0	-0.35
	0.0239	445137	7.52e-3	0.66	7.90e-5	1.60	1.10e-2	0.67	4.24e-0	-0.35	4.24e-0	-0.35
	0.1667	17569	2.17e-2	−−	9.88e-4	−−	3.14e-2	−−	2.32e-0	−−	2.32e-0	−−
	0.0927	58609	1.40e-2	0.75	3.67e-4	1.69	2.03e-2	0.74	2.74e-0	-0.28	2.74e-0	-0.28
2	0.0478	222913	8.86e-3	0.69	1.31e-4	1.55	1.29e-2	0.68	3.44e-0	-0.34	3.44e-0	-0.34
	0.0321	493057	6.80e-3	0.67	7.25e-5	1.49	9.93e-3	0.67	3.96e-0	-0.35	3.96e-0	-0.35
	0.0239	889585	5.59e-3	0.67	4.72e-5	1.45	8.17e-3	0.67	4.40e-0	-0.35	4.40e-0	-0.35

Table 5.5: Example 2, history of convergence using quadrilaterals.

k	h	N	$\mathtt{e}(\boldsymbol{\rho})$	$\mathtt{r}(\boldsymbol{\rho})$	$\mathtt{e}(\mathbf{u})$	$\mathtt{r}(\mathbf{u})$	$\mathtt{e}(\boldsymbol{\sigma})$	$\mathtt{r}(\boldsymbol{\sigma})$	$\mathtt{e}(\boldsymbol{\rho}^\star)$	$\mathtt{r}(\boldsymbol{\rho}^\star)$	$\mathtt{e}(\boldsymbol{\sigma}^\star)$	$\mathtt{r}(\boldsymbol{\sigma}^\star)$
	0.0672	9243	3.66e-2	−−	3.55e-2	−−	5.04e-2	−−	3.16e-0	−−	3.16e-0	−−
	0.0385	25483	2.63e-2	0.60	2.14e-2	0.91	3.63e-2	0.59	3.74e-0	-0.31	3.74e-0	-0.31
0	0.0275	49787	2.11e-2	0.65	1.53e-2	1.00	2.91e-2	0.65	4.19e-0	-0.33	4.19e-0	-0.33
	0.0214	82155	1.79e-2	0.66	1.19e-2	1.00	2.47e-2	0.65	4.55e-0	-0.33	4.55e-0	-0.33
	0.0170	129563	1.54e-2	0.66	9.45e-3	1.00	2.12e-2	0.66	4.91e-0	-0.33	4.91e-0	-0.33
	0.0672	27725	1.86e-2	−−	6.63e-4	−−	2.63e-2	−−	3.41e-0	−−	3.41e-0	−−
	0.0385	76445	1.32e-2	0.61	2.87e-4	1.50	1.87e-2	0.61	4.04e-0	-0.31	4.04e-0	-0.31
1	0.0275	149357	1.06e-2	0.67	1.65e-4	1.64	1.49e-2	0.67	4.52e-0	-0.33	4.52e-0	-0.33
	0.0214	246461	8.95e-3	0.67	1.10e-4	1.64	1.26e-2	0.67	4.92e-0	-0.33	4.92e-0	-0.33
	0.0170	388685	7.68e-3	0.67	7.51e-5	1.64	1.08e-2	0.67	5.31e-0	-0.33	5.31e-0	-0.33
	0.0672	53137	1.50e-2	−−	2.89e-4	−−	2.01e-2	−−	3.68e-0	−−	3.68e-0	−−
	0.0385	146517	1.07e-2	0.61	1.36e-4	1.36	1.43e-2	0.61	4.36e-0	-0.31	4.36e-0	-0.31
2	0.0275	286265	8.52e-3	0.67	8.34e-5	1.45	1.14e-2	0.67	4.88e-0	-0.33	4.88e-0	-0.33
	0.0214	472381	7.21e-3	0.67	5.83e-5	1.43	9.68e-3	0.67	5.30e-0	-0.33	5.30e-0	-0.33
	0.0170	744977	6.18e-3	0.67	4.21e-5	1.41	8.30e-3	0.67	5.72e-0	-0.33	5.72e-0	-0.33

Table 5.6: Example 2, history of convergence using hexagons.

k	h	N	$\mathtt{e}(\boldsymbol{\rho})$	$\mathtt{r}(\boldsymbol{\rho})$	$\mathtt{e}(\mathbf{u})$	$\mathtt{r}(\mathbf{u})$	$\mathtt{e}(\boldsymbol{\sigma})$	$\mathtt{r}(\boldsymbol{\sigma})$	$\mathtt{e}(\boldsymbol{\rho}^\star)$	$\mathtt{r}(\boldsymbol{\rho}^\star)$	$\mathtt{e}(\boldsymbol{\sigma}^\star)$	$\mathtt{r}(\boldsymbol{\sigma}^\star)$
	0.0643	4929	1.64e+1	−−	6.74e-1	−−	2.28e+1	−−	4.37e+1	−−	4.65e+1	−−
	0.0488	8527	1.24e+1	1.01	3.91e-1	1.97	1.73e+1	0.99	3.32e+1	1.00	3.53e+1	1.00
0	0.0248	32719	6.28e-0	1.01	1.02e-1	1.99	8.83e-0	1.00	1.69e+1	1.00	1.80e+1	1.00
	0.0166	72591	4.20e-0	1.00	4.60e-2	1.99	5.93e-0	1.00	1.13e+1	1.00	1.20e+1	1.00
	0.0129	121441	3.24e-0	1.00	2.75e-2	2.00	4.58e-0	1.00	8.73e-0	1.00	9.31e-0	1.00
	0.0643	17601	3.16e-1	−−	5.34e-3	−−	3.54e-1	−−	7.04e-1	−−	7.21e-1	−−
	0.0488	30509	1.83e-1	1.98	2.34e-3	2.98	2.05e-1	1.97	4.06e-1	2.00	4.16e-1	1.99
1	0.0248	117421	4.78e-2	1.99	3.11e-4	2.99	5.38e-2	1.98	1.05e-1	2.00	1.08e-1	2.00
	0.0166	260781	2.16e-2	1.99	9.42e-5	2.99	2.43e-2	1.99	4.74e-2	2.00	4.86e-2	2.00
	0.0129	436481	1.29e-2	1.99	4.36e-5	2.99	1.46e-2	1.99	2.83e-2	2.00	2.90e-2	2.00
	0.0643	36081	2.58e-3	−−	2.73e-5	−−	2.58e-3	−−	1.73e-3	−−	1.74e-3	−−
	0.0488	62583	1.13e-3	3.00	9.05e-6	4.00	1.13e-3	3.00	7.57e-4	3.00	7.59e-4	3.00
2	0.0248	241111	1.48e-4	3.00	6.09e-7	3.99	1.48e-4	3.00	9.96e-5	3.00	1.00e-4	3.00
	0.0166	535671	4.48e-5	3.00	1.24e-7	3.98	4.48e-5	3.00	3.00e-5	3.00	3.02e-5	3.00
	0.0129	896721	2.07e-5	3.00	4.45e-8	3.97	2.07e-5	3.00	1.39e-5	3.00	1.39e-5	3.00

Table 5.7: Example 3, history of convergence using triangles.

k	h	N	$\mathtt{e}(\boldsymbol{\rho})$	$\mathtt{r}(\boldsymbol{\rho})$	$\mathtt{e}(\mathbf{u})$	$\mathtt{r}(\mathbf{u})$	$\mathtt{e}(\boldsymbol{\sigma})$	$\mathtt{r}(\boldsymbol{\sigma})$	$\mathtt{e}(\boldsymbol{\rho}^\star)$	$\mathtt{r}(\boldsymbol{\rho}^\star)$	$\mathtt{e}(\boldsymbol{\sigma}^\star)$	$\mathtt{r}(\boldsymbol{\sigma}^\star)$
	0.0716	5521	1.91e+1	−−	9.06e-1	−−	1.99e+1	−−	5.42e+1	−−	5.44e+1	−−
	0.0537	9761	1.35e+1	1.20	4.69e-1	2.29	1.38e+1	1.26	3.91e+1	1.13	3.92e+1	1.14
0	0.0286	34051	6.70e-0	1.12	1.19e-1	2.18	6.74e-0	1.14	1.98e+1	1.08	1.98e+1	1.08
	0.0195	73041	4.47e-0	1.06	5.31e-2	2.10	4.48e-0	1.07	1.33e+1	1.04	1.33e+1	1.04
	0.0148	126731	3.36e-0	1.04	3.01e-2	2.06	3.36e-0	1.04	1.00e+1	1.03	1.00e+1	1.03
	0.0716	18241	5.22e-1	−−	7.03e-3	−−	5.26e-1	−−	1.34e-0	−−	1.35e-0	−−
	0.0537	32321	2.72e-1	2.27	2.68e-3	3.35	2.73e-1	2.28	6.94e-1	2.30	6.95e-1	2.30
1	0.0286	113101	6.92e-2	2.18	3.49e-4	3.24	6.93e-2	2.18	1.77e-1	2.18	1.77e-1	2.18
	0.0195	242881	3.10e-2	2.10	1.05e-4	3.13	3.10e-2	2.10	7.95e-2	2.09	7.95e-2	2.09
	0.0148	421661	1.75e-2	2.07	4.49e-5	3.08	1.75e-2	2.07	4.50e-2	2.06	4.50e-2	2.06
	0.0716	36361	8.87e-3	−−	3.27e-5	−−	8.88e-3	−−	7.51e-3	−−	7.53e-3	−−
	0.0537	64481	3.21e-3	3.54	7.77e-6	5.00	3.21e-3	3.54	2.69e-3	3.57	2.70e-3	3.57
2	0.0286	225901	3.99e-4	3.32	3.65e-7	4.86	3.99e-4	3.32	3.30e-4	3.34	3.30e-4	3.34
	0.0195	485321	1.19e-4	3.16	6.29e-8	4.59	1.19e-4	3.16	9.80e-5	3.17	9.80e-5	3.17
	0.0148	842741	5.03e-5	3.11	1.92e-8	4.30	5.03e-5	3.11	4.15e-5	3.11	4.15e-5	3.11

Table 5.8: Example 3, history of convergence using quadrilaterals.

k	h	N	$\mathtt{e}(\boldsymbol{\rho})$	$\mathtt{r}(\boldsymbol{\rho})$	$\mathtt{e}(\mathbf{u})$	$\mathtt{r}(\mathbf{u})$	$\mathtt{e}(\boldsymbol{\sigma})$	$\mathtt{r}(\boldsymbol{\sigma})$	$\mathtt{e}(\boldsymbol{\rho}^\star)$	$\mathtt{r}(\boldsymbol{\rho}^\star)$	$\mathtt{e}(\boldsymbol{\sigma}^\star)$	$\mathtt{r}(\boldsymbol{\sigma}^\star)$
	0.0414	8147	1.50e+1	−−	4.07e-1	−−	1.51e+1	−−	4.44e+1	−−	4.45e+1	−−
	0.0319	13563	1.16e+1	0.99	2.45e-1	1.95	1.17e+1	0.99	3.44e+1	0.99	3.44e+1	0.99
0	0.0235	24579	8.54e-0	1.00	1.34e-1	1.99	8.57e-0	1.01	2.54e+1	0.99	2.54e+1	0.99
	0.0167	48603	6.05e-0	1.00	6.73e-2	1.99	6.07e-0	1.00	1.81e+1	0.99	1.81e+1	1.00
	0.0124	88637	4.48e-0	1.00	3.70e-2	1.99	4.49e-0	1.00	1.34e+1	1.00	1.34e+1	1.00
	0.0414	24437	3.01e-1	−−	3.24e-3	−−	3.02e-1	−−	7.85e-1	−−	7.85e-1	−−
	0.0319	40757	1.81e-1	1.97	1.51e-3	2.93	1.81e-1	1.97	4.70e-1	1.98	4.70e-1	1.98
1	0.0235	73733	9.84e-2	1.99	6.10e-4	2.97	9.85e-2	1.99	2.56e-1	1.99	2.56e-1	1.99
	0.0167	145805	4.96e-2	1.99	2.19e-4	2.97	4.96e-2	1.99	1.29e-1	1.99	1.29e-1	1.99
	0.0124	266089	2.72e-2	1.99	8.98e-5	2.97	2.73e-2	1.99	7.07e-2	2.00	7.07e-2	2.00
	0.0414	46835	4.04e-3	−−	1.94e-5	−−	4.45e-3	−−	3.53e-3	−−	4.00e-3	−−
	0.0319	78175	1.87e-3	2.97	6.89e-6	3.98	2.06e-3	2.97	1.64e-3	2.97	1.85e-3	2.97
2	0.0235	141319	7.48e-4	2.99	2.04e-6	3.98	8.27e-4	2.99	6.55e-4	2.99	7.43e-4	2.99
	0.0167	279457	2.67e-4	2.99	5.18e-7	3.99	2.96e-4	2.99	2.34e-4	2.99	2.66e-4	2.99
	0.0124	510153	1.09e-4	2.99	1.56e-7	3.99	1.20e-4	2.99	9.52e-5	2.99	1.08e-4	2.99

Table 5.9: Example 3, history of convergence using hexagons.

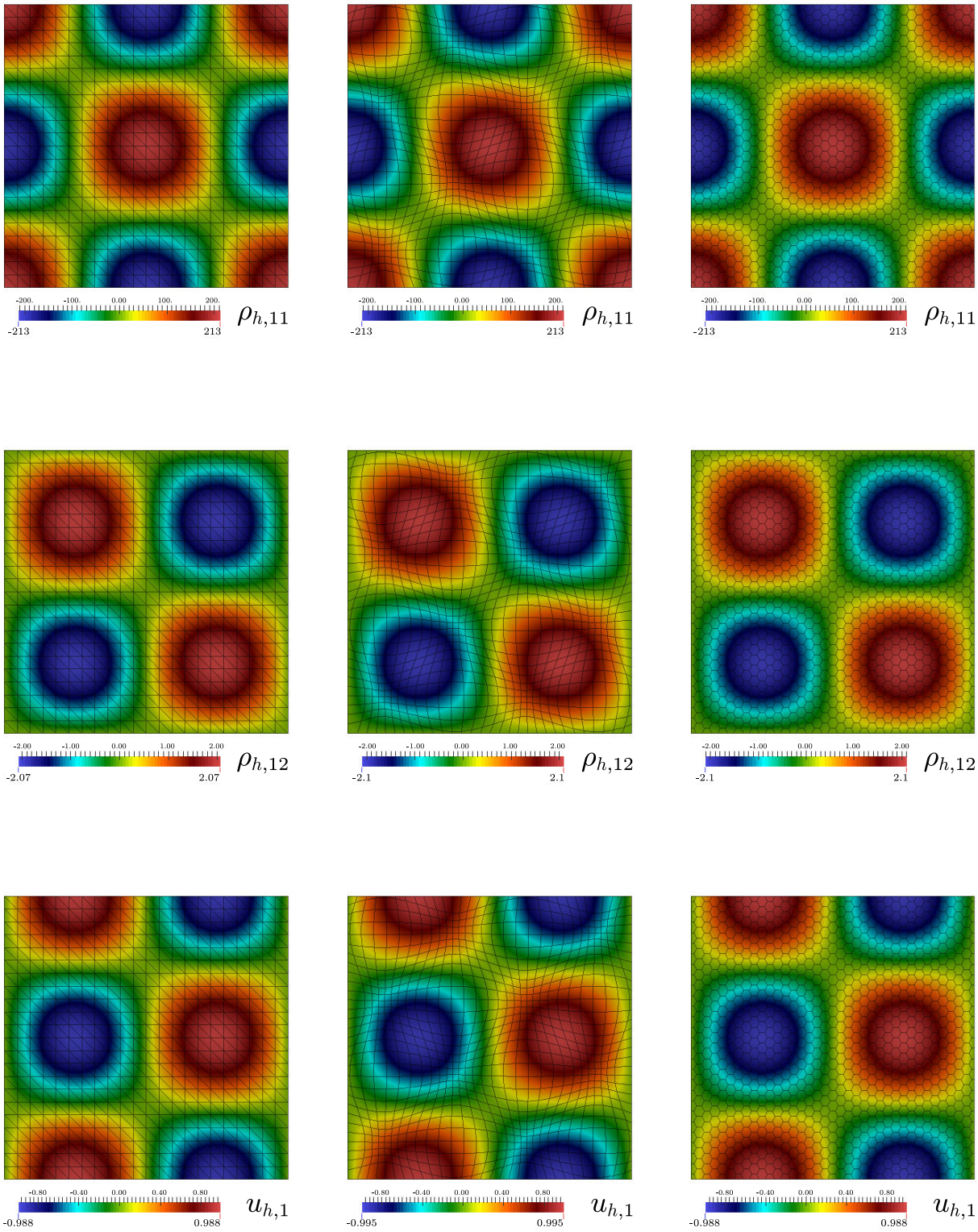

Figure 5.1: Example 1, $\rho_{h,11}$ (top), $\rho_{h,12}$ (center) and $u_{h,1}$ (bottom), using $k = 2$ and the first mesh of each kind (columns).

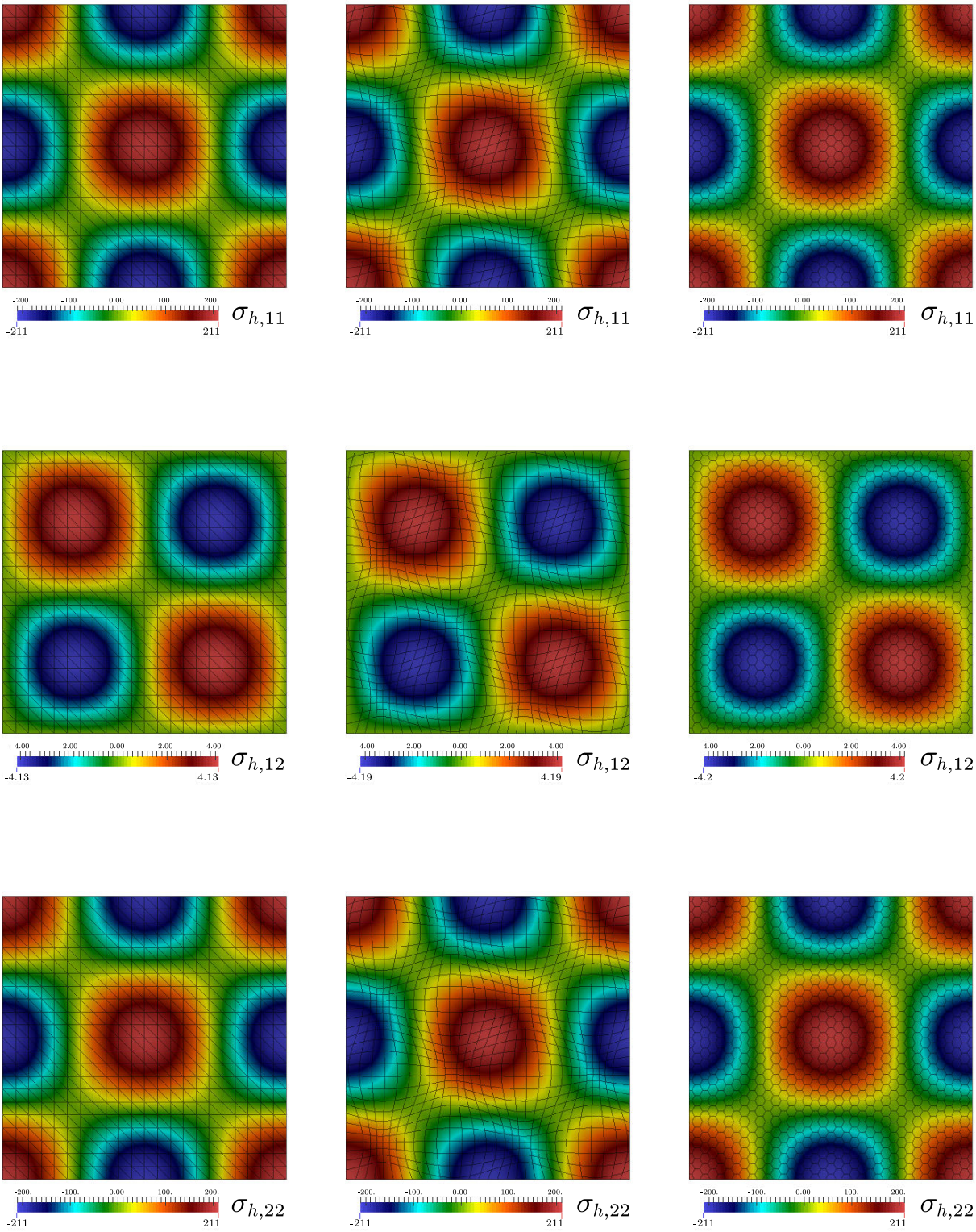

Figure 5.2: Example 1, $\sigma_{h,11}$ (top), $\sigma_{h,12}$ (center) and $\sigma_{h,22}$ (bottom), using $k = 2$ and the first mesh of each kind (columns).

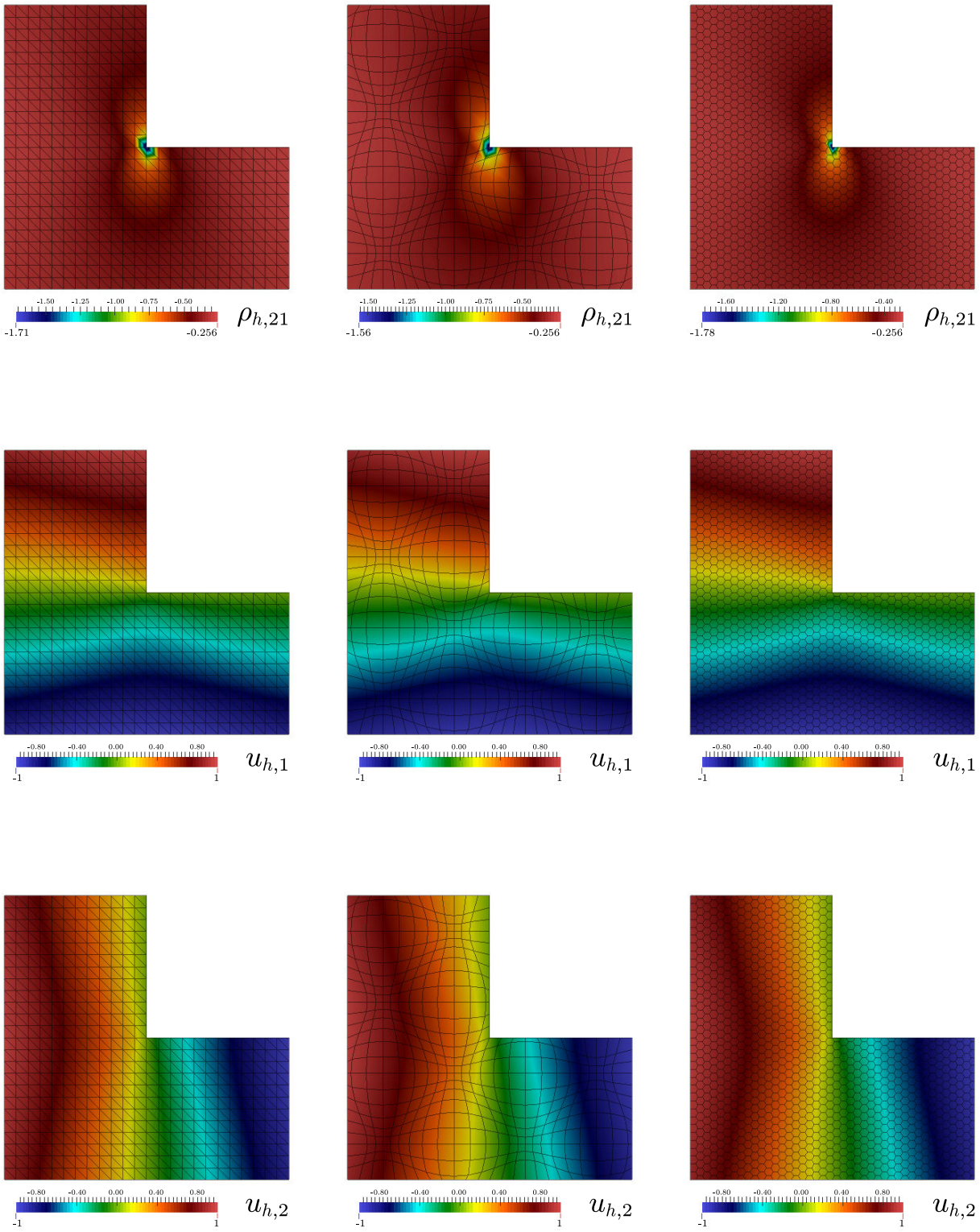

Figure 5.3: Example 2, $\rho_{h,21}$ (top), $u_{h,1}$ (center) and $u_{h,2}$ (bottom), using $k = 2$ and the first mesh of each kind (columns).

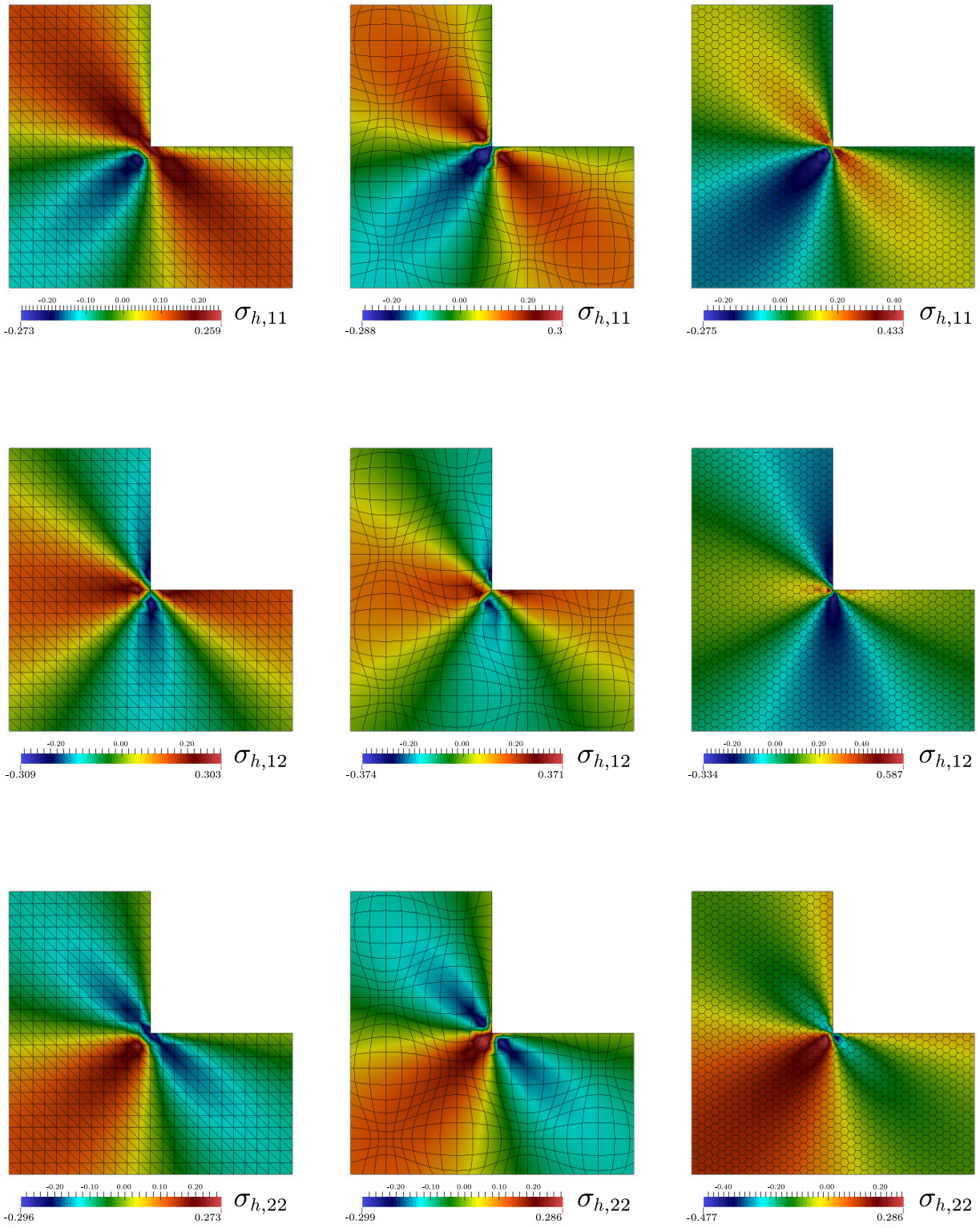

Figure 5.4: Example 2, $\sigma_{h,11}$ (top), $\sigma_{h,12}$ (center) and $\sigma_{h,22}$ (bottom), using $k = 2$ and the first mesh of each kind (columns).

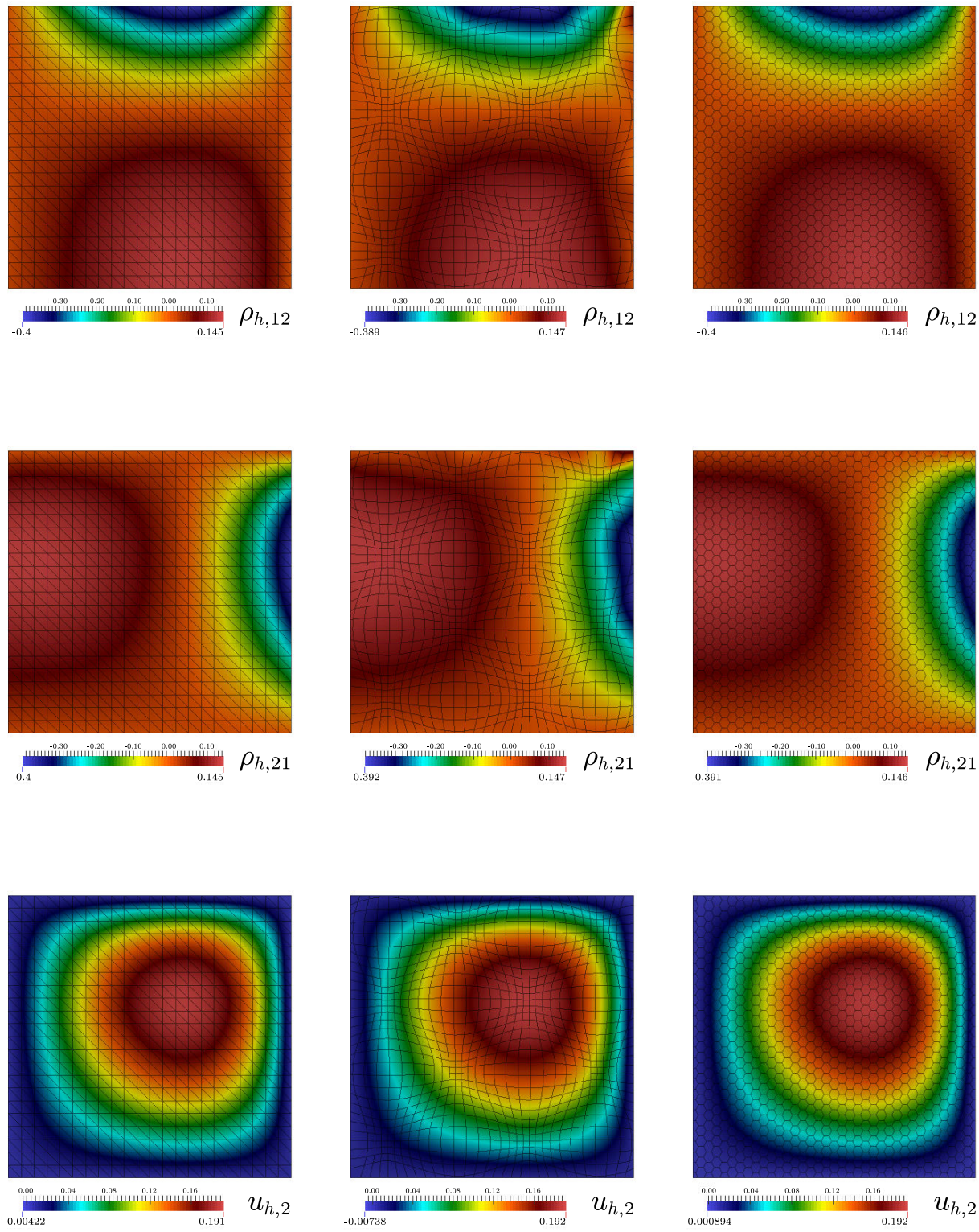

Figure 5.5: Example 3, $\rho_{h,12}$ (top), $\rho_{h,21}$ (center) and $u_{h,2}$ (bottom), using $k = 2$ and the first mesh of each kind (columns).

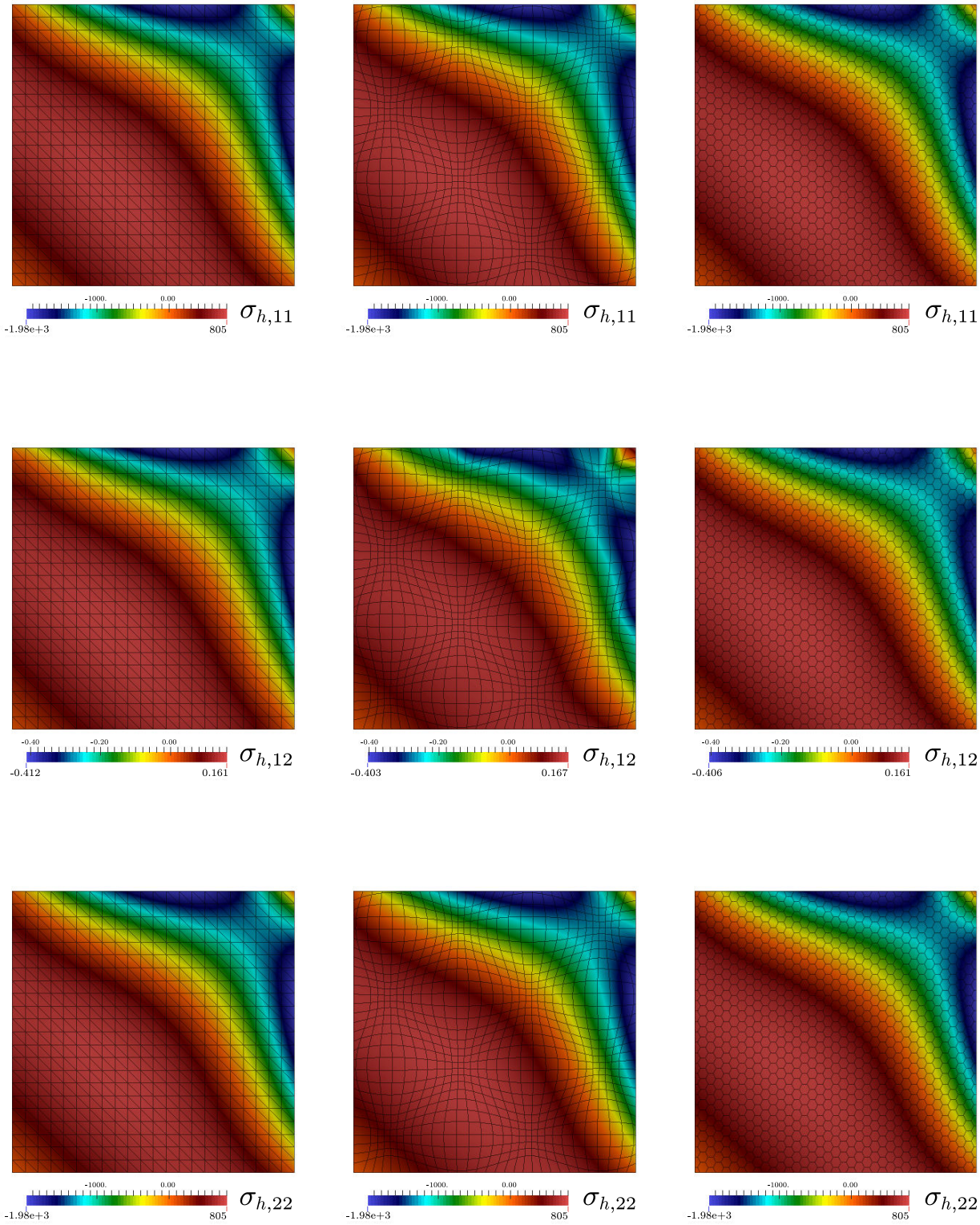

Figure 5.6: Example 3, $\sigma_{h,11}$ (top), $\sigma_{h,12}$ (center) and $\sigma_{h,22}$ (bottom), using $k = 2$ and the first mesh of each kind (columns).

References

[1] B. Ahmad, A. Alsaedi, F. Brezzi, L. D. Marini, and A. Russo, *Equivalent projectors for virtual element methods*, Comput. Math. Appl., 66 (2013), pp. 376–391.

[2] P. F. Antonietti, L. Beirão da Veiga, D. Mora, and M. Verani, *A stream virtual element formulation of the Stokes problem on polygonal meshes*, SIAM J. Numer. Anal, 52 (2014), pp. 386–404.

[3] E. Artioli, S. de Miranda, C. Lovadina, and L. Patruno, *A stress/displacement virtual element method for plane elasticity problems*, Comput. Methods Appl. Mech. Engrg., 325 (2017), pp. 155–174.

[4] L. Beirão da Veiga, F. Brezzi, A. Cangiani, L. D. Marini, G. Manzini, and A. Russo, *Basic principles of virtual elements methods*, Math. Models Methods Appl. Sci., 23 (2013), pp. 199–214.

[5] L. Beirão da Veiga, F. Brezzi, and L. D. Marini, *Virtual elements for linear elasticity problems*, SIAM J. Numer. Anal., 51 (2013), pp. 794–812.

[6] L. Beirão da Veiga, F. Brezzi, L. D. Marini, and A. Russo, *$H(div)$ and $H(curl)$-conforming VEM*, Numer. Math., 133 (2016), pp. 303–332.

[7] ——, *Mixed virtual element methods for general second order elliptic problems on polygonal meshes*, ESAIM Math. Model. Numer. Anal., 50 (2016), pp. 727–747.

[8] ——, *Virtual element methods for general second-order elliptic problems on polygonal meshes*, Math. Models Methods Appl. Sci., 26 (2016), pp. 729–750.

[9] L. Beirão da Veiga, C. Lovadina, and G. Vacca, *Divergence free virtual elements for the Stokes problem on polygonal meshes*, ESAIM Math. Model. Numer. Anal., 51 (2017), pp. 509–535.

[10] L. Beirão da Veiga, C. Lovadina, and G. Vacca, *Virtual elements for the Navier-Stokes problem on polygonal meshes*, arXiv:1703.00437v2 [math.NA], (2017).

[11] F. Brezzi, R. S. Falk, and L. D. Marini, *Basic principles of mixed virtual element methods*, ESAIM Math. Model. Numer. Anal., 48 (2014), pp. 1227–1240.

[12] F. Brezzi and L. D. Marini, *Virtual element methods for plate bending problems*, Comput. Methods Appl. Mech. Engrg., 253 (2013), pp. 455–462.

[13] E. Cáceres and G. N. Gatica, *A mixed virtual element method for the pseudostress-velocity formulation of the Stokes problem*, IMA J. Numer. Anal., 37 (2017), pp. 296–331.

[14] E. Cáceres, G. N. Gatica, and F. A. Sequeira, *A mixed virtual element method for the Brinkman problem*, Math. Models Methods Appl. Sci., 27 (2017), pp. 707–743.

[15] ——, *A mixed virtual element method for quasi-Newtonian Stokes flows*, SIAM J. Numer. Anal., 56 (2018), pp. 317–343.

[16] A. L. Gain, C. Talischi, and G. H. Paulino, *On the virtual element method for three-dimensional linear elasticity problems on arbitrary polyhedral meshes*, Comput. Methods Appl. Mech. Engrg, 282 (2014), pp. 132–160.

[17] G. N. Gatica, *Analysis of a new augmented mixed finite element method for linear elasticity allowing $\mathbb{RT}_0 - \mathbb{P}_1 - \mathbb{P}_0$ approximations*, ESAIM Math. Model. Numer. Anal., 40 (2006), pp. 1–28.

[18] G. N. Gatica, L. F. Gatica, and A. Márquez, *Analysis of a pseudostress-based mixed finite element method for the Brinkman model of porous media flow*, Numer. Math., 126 (2014), pp. 635–677.

[19] G. N. Gatica, L. F. Gatica, and F. A. Sequeira, *Analysis of an augmented pseudostress-based mixed formulation for a nonlinear Brinkman model of porous media flow*, Comput. Methods Appl. Mech. Engrg., 289 (2015), pp. 104–130.

[20] ——, *A* $\mathbb{RT}_k - \mathbf{P}_k$ *approximation for linear elasticity yielding a broken* $\mathbb{H}(\mathbf{div})$ *convergent post-processed stress*, Appl. Math. Lett, 49 (2015), pp. 133–140.

[21] ——, *A priori and a posteriori error analyses of a pseudostress-based mixed formulation for linear elasticity*, Comput. Math. Appl., 71 (2016), pp. 585–614.

[22] G. N. Gatica, A. Márquez, and S. Meddahi, *An augmented mixed finite element method for 3D linear elasticity problems*, J. Comput. Appl. Math., 231 (2009), pp. 526–540.

[23] G. N. Gatica, A. Márquez, and M. A. Sánchez, *A priori and a posteriori error analyses of a velocity-pseudostress formulation for a class of quasi-Newtonian Stokes flows*, Comput. Methods Appl. Mech. Engrg., 200 (2011), pp. 1619–1636.

[24] G. N. Gatica, M. Munar, and F. A. Sequeira, *A mixed virtual element method for a nonlinear Brinkman model of porous media flow*, Preprint 2017-32, Centro de Investigación en Ingeniería Matemática, Universidad de Concepción, Chile, (2017).

[25] ——, *A mixed virtual element method for the Navier-Stokes equations*, Preprint 2017-23, Centro de Investigación en Ingeniería Matemática, Universidad de Concepción, Chile, (2017).